Rapid Miocene slip on the Snake Range–Deep Creek Range fault system, east-central Nevada

Elizabeth L. Miller* } *Department of Geological and Environmental Sciences, Stanford University,*
Trevor A. Dumitru } *Stanford, California 94305*

Roderick W. Brown† *Victorian Institute of Earth and Planetary Sciences, La Trobe University, Bundoora, Victoria 3083, Australia*

Phillip B. Gans *Department of Geological Sciences, University of California, Santa Barbara, California 93106*

ABSTRACT

New fission-track data together with 1:24 000-scale geologic mapping and analysis of Tertiary sedimentary deposits provide better constraints on the time and nature of motion along the Snake Range décollement, a classic Basin and Range metamorphic core complex detachment fault in east-central Nevada. Here, the fission-track method provides a particularly effective tool for dating faulting where bracketing or crosscutting relations are not available. These new data suggest that the Snake Range décollement forms part of a more extensive, 150-km-long north-south–trending fault system, the Snake Range–Deep Creek Range fault system. This fault system extends along the eastern flank of the northern and southern Snake Range, Kern Mountains, and Deep Creek Range, and accommodated at least 12–15 km of rapid slip in the Miocene, ca. 17 Ma. This component of motion is distinctly younger (by about 15–20 m.y.) than an earlier episode of slip and extension across the region bracketed stratigraphically and geochronologically as late Eocene–early Oligocene age.

Apatite fission-track ages (n = 57) in most parts of the Snake Range and adjacent ranges cluster at 17 Ma, indicating rapid cooling from >125 to <50 °C during exhumation at that time. In the northern Snake Range, zircon fission-track ages (n = 3) are essentially concordant with the apatite ages, indicating very rapid cooling from >310 to <50 °C. Formation of at least part of the pervasive mylonitic fabrics in the northern Snake Range may have occurred during this Miocene time interval, very late rather than early in the extensional history of the region. Coarse fanglomerate and rock-avalanche deposits in flanking Tertiary basins provide additional evidence for major tectonism at this time. Comparison of the timing of events in the northern Snake Range to that along strike of the fault system indicates that Miocene slip along the low-angle northern Snake Range décollement and exhumation of extensive footwall mylonites were coeval with more typical Basin and Range high-angle rotational faulting in the Deep Creek Range and Kern Mountains to the north and in the southern Snake Range to the south. This suggests that the two styles of faulting (low-angle detachment and high-angle rotational) can occur simultaneously along the length of a single normal fault system. Data from the northern Snake Range also underscore the importance of a vertical component of uplift of the range in Miocene time, leading to the present domal geometry of the northern Snake Range décollement.

When considered together with footwall deformational fabrics, the new data are most simply explained as the consequence of higher local geothermal gradients and a shallower brittle-ductile transition zone along the northern Snake Range part of the fault system. It can be speculated that the Snake Range metamorphic core complex represents the top of a stretching welt of hotter, deeper level crust that rose during extension. This rising welt may have been localized by the presence of previously thickened crust beneath the region and could have been triggered by increased regional magmatism and heating accompanying rapid extension in Miocene time.

INTRODUCTION

The northern Snake Range in east-central Nevada (Fig. 1) is a classic example of a normal fault-bounded metamorphic core complex developed as a consequence of Tertiary extension of the Basin and Range province (e.g., Coney, 1979). A suite of 13 geologic quadrangle maps for the region depict in detail the bounding low-angle detachment fault system, the Snake Range décollement (Miller et al., 1994b, 1999a, 1999b; McGrew and Miller, 1995; Miller and Grier, 1995; Gans et al., 1999, in press; Lee et al., 1999a, 1999b, 1999c; Miller and Gans, 1999). Although closely studied, the origin and tectonic significance of the Snake Range décollement remain enigmatic. Named and first interpreted as a Mesozoic thrust fault by Misch (1960), it has been reinterpreted as a brittle-ductile transition zone developed during extension (Miller et al., 1983), as a low-angle fault with considerable displacement (Bartley and Wernicke, 1984), as a combination of a brittle-ductile transition and shear zone with less displacement (Lee et al., 1987), and as an example of a rolling hinge normal fault (Buck, 1988; Lee, 1995).

This paper discusses the timing of exhumation and cooling of the footwall of this metamorphic core complex detachment fault based on fission-track dating and the record of this uplift as preserved in synextensional sedimentary rocks. Although the origin of this low-angle detachment fault system remains problematic, our new data indicate that extensional strain along this detachment system was coeval with large displacements along the Deep Creek Range and Kern Mountains faults to the north and along the southern Snake Range décollement to the south. Both are regions of somewhat less Miocene strain where high-angle rotational faulting played a key role in

*E-mail: miller@pangea.stanford.edu.

†Present address: School of Earth Sciences, University of Melbourne, Parkville, Victoria 3052, Australia.

GSA Bulletin; June 1999; v. 111; no. 6; p. 886–905; 10 figures; 1 table.

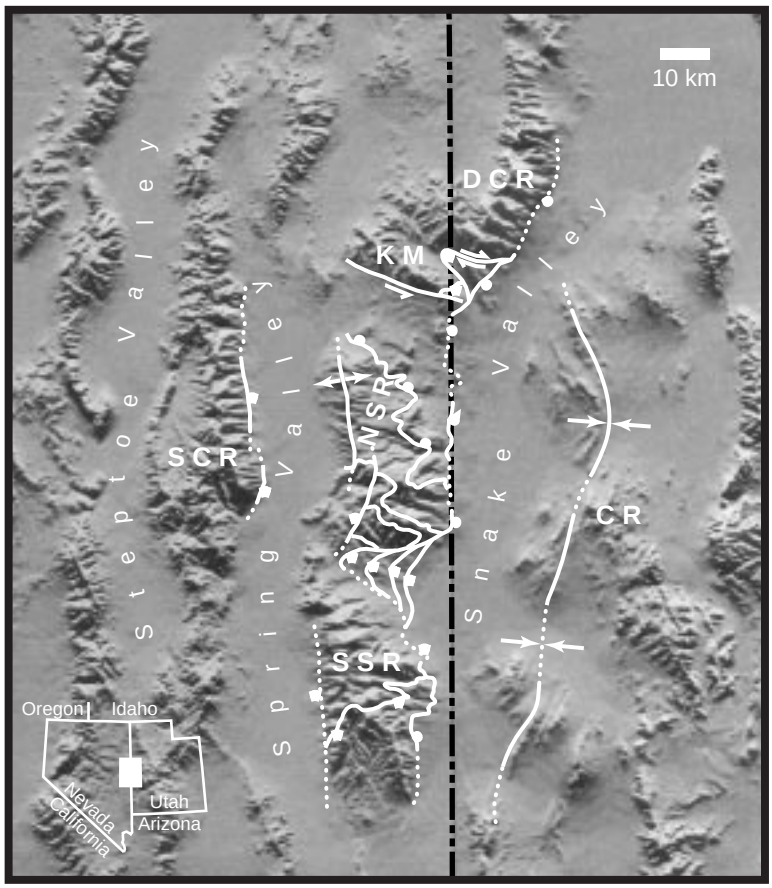

Figure 1. Digital relief map of east-central Nevada showing locations of the mountain ranges discussed in this paper: SSR—southern Snake Range; NSR—northern Snake Range; DCR—Deep Creek Range; SCR—Schell Creek Range; KM—Kern Mountains; CR—Confusion Range. The east-dipping Snake Range–Deep Creek Range normal fault system defines the eastern flank of these ranges and was responsible for the exhumation of the footwall rocks in the ranges, mostly in Miocene time. Tertiary sediments were deposited and preserved within transverse zones of deformation between the ranges (e.g., Sacramento Pass basin). Digital base map is from Edwards and Batson (1990a, 1990b).

unroofing footwall rocks. Indirectly, this comparison provides new perspectives on the nature of low-angle metamorphic core complex detachment faults and suggests that the observed differences in footwall deformation along strike of this fault system may be related to greater local Miocene heating and crustal flow beneath the northern Snake Range.

FISSION-TRACK ANALYSIS

Apatite fission-track analysis is a particularly effective tool for directly dating the exhumation and cooling of footwall rocks that accompany major normal fault slip in the brittle crust (Fig. 2). Gans et al. (1991) modeled the thermal evolution of the footwall and hanging wall during normal fault slip and concluded that fission-track cooling ages of samples collected from the footwall within several kilometers of the overlying normal fault system can be used to directly date the time of uplift and exhumation related to this slip. Essentially, rocks from this part of the footwall move relatively up and out from beneath the hanging wall during major fault slip, causing exhumation and cooling that can be dated by the fission-track method (Fig. 2C). Many studies have now utilized this general approach with excellent results (e.g., Foster et al., 1990; Fitzgerald et al., 1991; John and Foster, 1993; John and Howard, 1995; Howard and Foster, 1996; Dumitru et al., 1997). Figure 2 illustrates the basic aspects of this approach for the study of high-angle rotational faults. Because fission tracks in apatite anneal (are erased) completely above 110–125 °C (e.g., Green et al., 1989a, 1989b), rocks would be exhumed by faulting from sufficient depths (4–5 km) if, for example, slip on 60° dipping faults were at least 5 km given a geothermal gradient of 25 °C/km (Fig. 2). Rapid average slip rates (e.g., >2 km/m.y.) would result in near-concordant apatite ages and long track-length distributions over the portion of the footwall exhumed from hotter than 100–125 °C during this period of slip (Fig. 2F) (e.g., Green et al., 1989b). Structurally above this zone of near-concordant ages would be a zone of systematically older ages representing the exhumed partial annealing zone, where tracks were not completely erased before exhumation (Fig. 2F). The horizontal distance across the exhumed totally annealed section may be added to the inferred thickness of the nonannealed and partially annealed section (nominally about 4 km assuming a typical 25 °C/km geothermal gradient) to obtain a minimum estimate of the amount of horizontal extension (Fig. 2C). This simple approach is compromised if additional heat sources such as magmatism were present, if more than one major fault were superimposed, or if significant redistribution of heat occurred by mass flow of footwall rocks. Because all of these factors may play important roles in generating the ultimate geometry of the more controversial low-angle metamorphic core complex detachment faults, the approach shown in Figure 2 may not be directly applicable to such fault systems. Even in these circumstances, however, the array of fission-track ages still bear on the specific time and rate of exhumation leading to the cooling of the samples in question.

GEOLOGIC SETTING

The Snake Range and surrounding mountain ranges are underlain primarily by an upper Precambrian to Triassic miogeoclinal shelf sequence deposited along the western continental margin of North America (Fig. 3). Deposition ceased and these units were gently folded during regional metamorphism and intrusion of plutons at depth in Mesozoic time (Miller et al., 1988). The Precambrian to Triassic stratigraphic succession has been studied extensively and provides exceptional structural control on subsequent extension-related faulting in the region (e.g., Gans and Miller, 1983; Miller et al., 1983). Information discussed in the following suggests that the northern Snake Range décollement forms part of a more extensive 150-km-long fault system, here termed the Snake Range–Deep Creek Range fault system, which moved first in Eocene-Oligocene time, and then again in Miocene time, ca. 17 Ma. This single fault system, depicted in Figure 3, serves, on a regional scale, to uplift the deeper Precambrian and Cambrian parts of the miogeoclinal succession (which compose the footwall to this fault system) relative to upper Paleozoic units. These older footwall units now underlie the highest peaks of the region in the north-

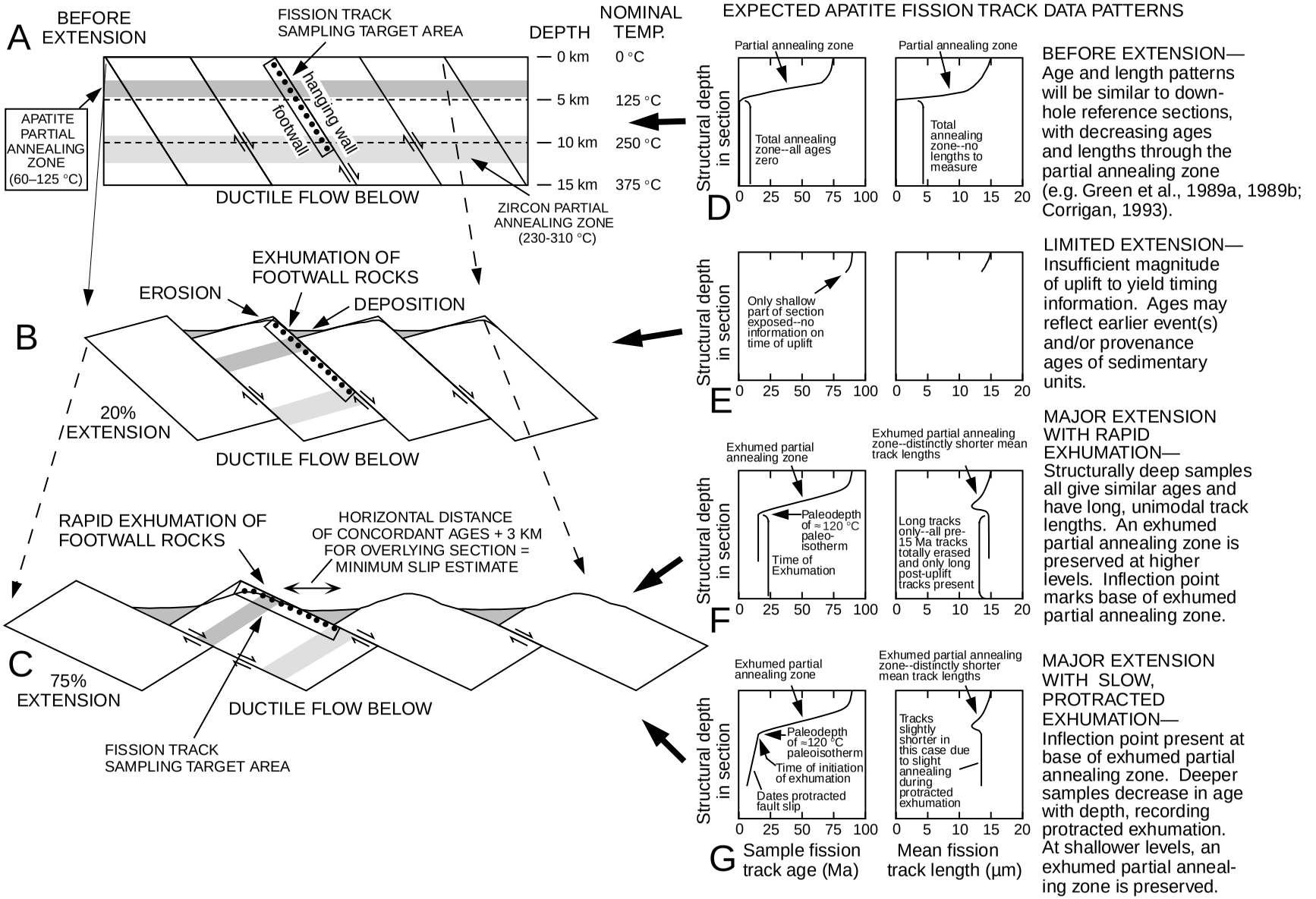

BEFORE EXTENSION—Age and length patterns will be similar to down-hole reference sections, with decreasing ages and lengths through the partial annealing zone (e.g. Green et al., 1989a, 1989b; Corrigan, 1993).

LIMITED EXTENSION—Insufficient magnitude of uplift to yield timing information. Ages may reflect earlier event(s) and/or provenance ages of sedimentary units.

MAJOR EXTENSION WITH RAPID EXHUMATION—Structurally deep samples all give similar ages and have long, unimodal track lengths. An exhumed partial annealing zone is preserved at higher levels. Inflection point marks base of exhumed partial annealing zone.

MAJOR EXTENSION WITH SLOW, PROTRACTED EXHUMATION—Inflection point present at base of exhumed partial annealing zone. Deeper samples decrease in age with depth, recording protracted exhumation. At shallower levels, an exhumed partial annealing zone is preserved.

Figure 2. Schematic diagrams illustrating how apatite fission-track ages and track lengths can be used to date the exhumation and cooling of footwall rocks that occur by normal faulting during crustal extension. Large amounts of fault slip and block rotation (C) tectonically exhume and expose rocks that formerly resided in the apatite fission-track total annealing (erasure) zone at temperatures hotter than about 100–125 °C. Apatite ages of such rocks date the time of exhumation and fault slip (F and G). Higher level samples from the partial annealing zone exhibit systematically older ages and shorter mean track lengths, due to incomplete erasure of tracks that formed before the exhumation event. Similarly, zircons exhumed from the zircon total erase zone (hotter than ~310 °C) also date fault slip (C). Note that multiple major faults, additional heat sources related to magmatism, or nonrigid behavior and flow of footwall rocks could compromise the utility of this simplistic approach. Sampling arrays in the footwall should be collected close to the projected plane of the fault (A–C) because the cooling history of rocks deeper in the fault block may be more complex and not as easy to relate directly to fault slip (Gans et al., 1991).

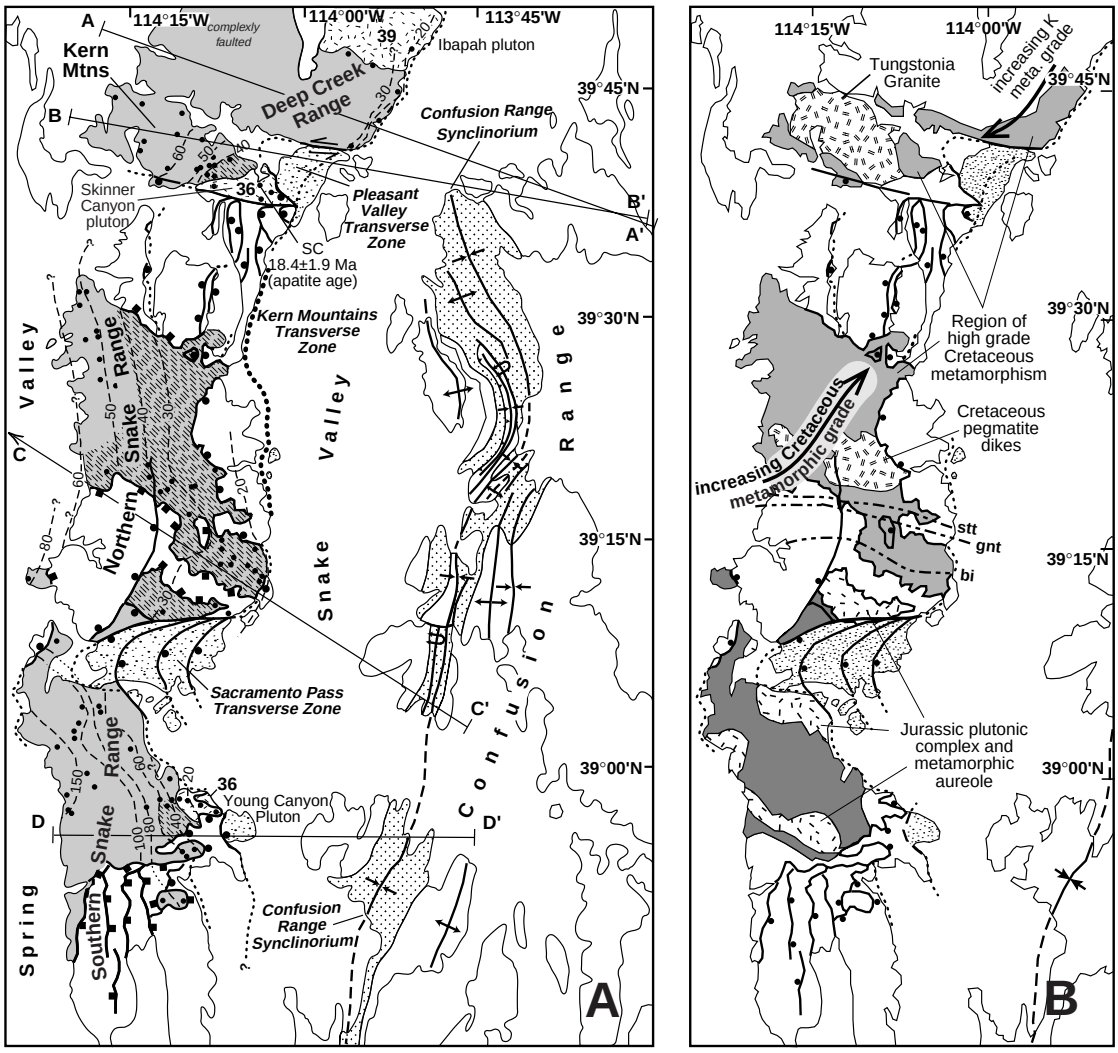

Tertiary features of footwall block

Footwall

- Extent of Tertiary ductile deformation (dashes show stretching lineations)
- 36 Tertiary plutons with U-Pb zircon ages shown
- Precambrian-Paleozoic strata and Mesozoic plutons
- K-Ar and $^{40}Ar/^{39}Ar$ white mica sample localities
- Contours of K-Ar and $^{40}Ar/^{39}Ar$ white mica total gas ages (Ma)

Hanging Wall

- Tilted Tertiary sediments
- Upper Paleozoic to Triassic miogeoclinal strata in Confusion Range
- Paleozoic miogeoclinal strata, undifferentiated (includes local Tertiary strata)
- Interpreted older portions of Snake Range décollement
- Younger normal fault systems and interpreted younger portions of Snake Range décollement
- Mesozoic thrust faults
- Folds

Mesozoic features of footwall block

- Tertiary sedimentary rocks
- Cretaceous plutons and pegmatite dikes
- Rocks metamorphosed in Cretaceous time
- Rocks metamorphosed in Jurassic time
- Jurassic plutonic complexes
- Paleozoic strata, undifferentiated
- Normal fault systems, undifferentiated
- Folds
- Metamorphic isograds

0 25 50 km

Figure 3. Simplified tectonic maps of the Snake Range, Kern Mountains, and Deep Creek Range. (A) Map emphasizing Cenozoic attributes of footwall rocks of the Cenozoic Snake Range–Deep Creek Range fault system that bounds these ranges on their eastern flank. Note eastward bulge in the Mesozoic Confusion Range synclinorium opposite the northern Snake Range, likely representing the region of greatest total Cenozoic extension across the fault system. Contours of K-Ar and $^{40}Ar/^{39}Ar$ total gas ages and the intrusive ages of igneous rocks are from the compilation of Miller et al. (1988). (B) Map emphasizing the along-strike continuity and similarities in the Mesozoic history of footwall rocks.

ern and southern Snake Range and in the Deep Creek Range, whereas upper Paleozoic hanging-wall strata underlie the relatively low-lying and unextended Mesozoic Confusion Range synclinorium to the east (Figs. 3 and 4). Within the fault system, Paleozoic hanging-wall units are cut, tilted, and attenuated by complex arrays of normal faults, particularly in the northern and southern Snake Range. Palinspastic restoration of structural cross sections suggests that the greatest amount of extension occurred across the northern Snake Range part of the fault system, where the most extensive footwall mylonites are developed and where the axis of the Confusion Range synclinorium is displaced farthest to the east (Miller et al., 1983; Gans and Miller, 1983) (Fig. 3). Total extension is less in the southern Snake Range to the south (McGrew, 1993) and in the Deep Creek Range to the north (Rodgers, 1987). Highly simplified sketches of the cross-sectional geometry of this fault system are shown in Figure 4. Transverse zones of deformation are present between each of the main mountain ranges that form the footwall to this fault system and appear to dictate the location or aid in the preservation of Tertiary sedimentary sequences (Fig. 3). These Tertiary sequences are bound on the north and south along the range fronts by faults with strike slip as well as normal components of displacement (Fig. 3).

Here we first highlight aspects of the Mesozoic history of the footwall rocks that enable us to establish the pre-Cenozoic structural continuity of this block along its entire length, from the southern Snake Range to the Deep Creek Range. The subsequent discussion of the Cenozoic history emphasizes the very different Cenozoic strain histories in different parts of the footwall. The fission-track data provide additional strong support for this inferred pre-Cenozoic footwall continuity.

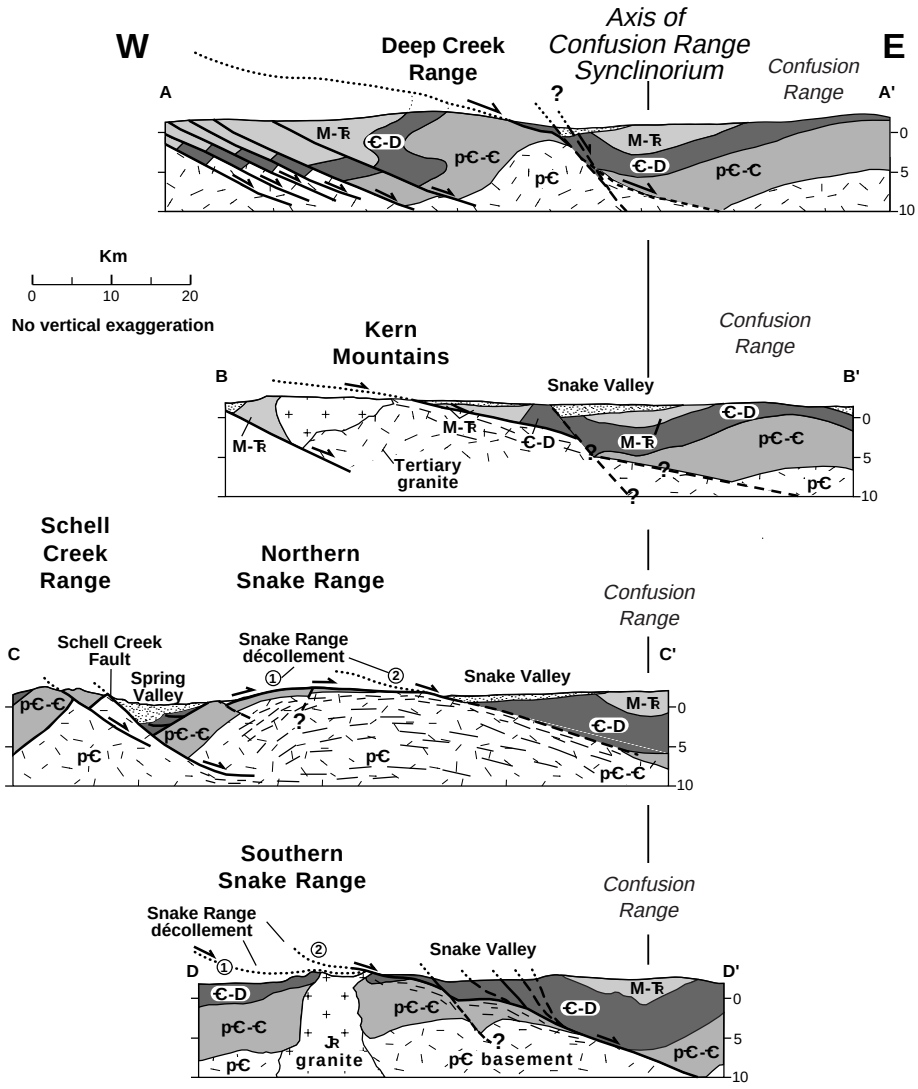

Figure 4. Schematic cross sections across the Snake Range–Deep Creek Range fault system based on interpretations of previous workers: (A) Rodgers (1987); (B) Smith et al. (1991); (C) Gans and Miller (1985); (D) McGrew (1993). Short lines represent approximate location and orientation of mylonitic foliation. Section locations are shown in Figure 5A.

MESOZOIC HISTORY OF FOOTWALL ROCKS

Good evidence exists for the original continuity of upper Precambrian to Cambrian units within the footwall block of the Snake Range–Deep Creek Range fault system, despite the obscuring effects of superimposed Cenozoic deformation (Figs. 3A, 4, and 5). In the southern Snake Range, upper Precambrian and Cambrian strata are weakly deformed and variably metamorphosed adjacent to Jurassic plutons dated as 160 Ma (Miller et al., 1988) (Figs. 3B and 5). These strata were once continuous with coeval strata immediately north of Sacramento Pass in the strongly deformed footwall of the northern Snake Range (Figs. 3B and 5). One of the key correlations is a quartzite unit in the Precambrian McCoy Creek Group (unit pCmc1 of Miller et al., 1994b) that exhibits rapid lateral facies variations. In the southern Snake Range south of Wheeler Peak, this unit is a massive cliff-forming quartzite. It becomes much thinner and conglomeratic north of Wheeler Peak. In its northernmost exposures in the southern Snake Range, it is a thin, distinctive quartz and chert pebble conglomerate. It is exposed across Sacramento Pass within a roof pendant in Jurassic plutonic rocks. Although more metamorphosed and deformed, it is still an easily recognized thin pebble conglomerate. This unit becomes a massive cliff-forming quartzite in exposures in Hendrys Creek farther north in the northern Snake Range (Miller et al., 1999; Miller and Gans, 1999). Other key correlations include the similarity in composition and age of Jurassic plutons (Fig. 3B) and the identical stratigraphy of the Cambrian Pole Canyon Limestone (which also exhibits fairly rapid facies variations in a north-south direction) on either side of Sacramento Pass. Within the northern Snake Range, upper Precambrian and Cambrian units, although strongly mylonitized, display map continuity throughout the range (Figs. 3 and 5). Thus, now-mylonitized footwall units of the northern Snake Range were once continuous with unmylonitized footwall units in the southern Snake Range.

Jurassic metamorphic fabrics in the southern part of the northern Snake Range are succeeded northward by Cretaceous metamorphic and defor-

mational fabrics (Fig. 3B). A series of mineral-in isograds related to the Cretaceous metamorphic event indicate steadily increasing metamorphic grade northward (Fig. 3B). Swarms of pegmatite dikes (now transposed by deformation to subhorizontal sill-like bodies) are present in the Smith Creek region and yield monazite U-Pb ages of 82 Ma. Nearby metamorphic rocks yield similar monazite ages of 78 Ma (Huggins and Wright, 1989; Huggins, 1990). In the northernmost reaches of the Snake Range, even units relatively high in the stratigraphic succession (e.g., Upper Cambrian and Ordovician) are metamorphosed to upper greenschist grade.

Due to lack of exposure, footwall units cannot be traced continuously northward across the Kern Mountains transverse zone into the Kern Mountains. However, Cretaceous plutonic rocks (the 75 Ma Tungstonia pluton; (Lee et al., 1986) and Paleozoic strata metamorphosed in the Cretaceous are exposed in a footwall position in the Kern Mountains (Fig. 3B). These Cretaceous metamorphic rocks can be mapped northward across the west end of Pleasant Valley (Fig. 3) into the main region of exposure of late Precambrian and Cambrian rocks in the Deep Creek Range, where they were also involved in Late Cretaceous deformation and metamorphism (Miller et al., 1988; Rodgers, 1987). A point of interest is that across the northern Snake Range and the Kern Mountains, higher Miocene temperatures and possibly mylonite development seem to be superimposed on rock sequences that have all undergone peak metamorphism in Late Cretaceous time. Although earlier Oligocene plutons are present in the Deep Creek Range, Kern Mountains, and southern Snake Range, they do not appear to have been the main source of heat for the bulk of the Tertiary metamorphism in the northern Snake Range.

In summary, footwall units of the Snake Range–Deep Creek Range fault system have a common depositional, metamorphic, and intrusive history that supports the conclusion that they formed a coherent tract of rocks at least 150 km long from north to south prior to disruption by Cenozoic deformation. This structural continuity is further supported by the similarities in higher temperature cooling histories based on K-Ar and total gas $^{40}Ar/^{39}Ar$ ages (Fig. 3A) and especially by the similarities in apatite fission-track ages we discuss below.

CENOZOIC HISTORY OF FOOTWALL ROCKS

The following discussion highlights key aspects of the Cenozoic deformational history of footwall rocks, the timing constraints on the age of mylonitic fabrics, and fission-track data that bear on the timing of exhumation, cooling, and fault slip along the Snake Range–Deep Creek Range fault system. Constraints on the age of faulting provided by Tertiary sedimentary successions add weight to our conclusions based on the thermochronologic database. Our discussion begins with the southern Snake Range, proceeds to the northern Snake Range where our data are most extensive, and then lesser data from the Schell Creek Range, Kern Mountains, and Deep Creek Range. Figures 5, 6, 7, 8, and 9 summarize timing constraints along the entire length of the fault system.

Fission-Track Principles and Methods

For this study, apatite and zircon from footwall quartzites, schists, and granitic rocks were analyzed using fission-track methods (Fig. 5 and Table 1). The use of apatite data for reconstructing thermal, burial, and unroofing histories relies on the fact that new ^{238}U fission tracks form at an essentially constant rate and with an essentially constant initial track length, while tracks are simultaneously annealed (erased) by elevated subsurface temperatures (e.g., Green et al., 1989a, 1989b; Dumitru, 1999). At temperatures hotter than 110–125 °C, annealing is total, erasing all tracks and resetting the fission-track clock to zero. If such samples then cool rapidly to temperatures cooler than about 50 °C, such as during exhumation, their fission-track ages will directly date the time of cooling (Fig. 2F). Where initial temperatures are cooler than 110–125 °C, such as at shallower levels in the crust, annealing is partial, which reduces apparent ages and track lengths but does not reset the fission-track clock completely to zero. If such samples cool during unroofing, the observed fission-track ages will be older than the time of cooling and the track length distributions will exhibit a significant component of short tracks that formed and were only partially annealed before the cooling event. Thus, observed ages and track lengths will vary systematically with former sample depth, as outlined in Figure 2, D–G.

Fission tracks in zircon anneal at higher temperatures than those in apatite and thus constrain higher temperature parts of the cooling history. The exact annealing temperatures for zircon are currently less well calibrated than for apatite. As summarized in Tagami and Dumitru (1996), we prefer a zircon annealing window of 230 °C (essentially no annealing) to 310 °C (total annealing) for a heating duration of the order of 10 m.y., and will assume those values for this study.

The horizontal distance that exposes totally reset samples in the tilted footwall of a fault block may be added to the inferred thickness of the overlying unreset and partially reset section to obtain a minimum estimate of the amount of slip during the time interval in question (Fig. 2C). In the estimates of fault slip from apatite data presented here, we conservatively assume a high preextension geothermal gradient of about 35 °C/km, leading to a conservative nominal thickness of about 3 km for the overlying section.

Southern Snake Range

The southern Snake Range is underlain by gently arched or domed upper Precambrian and Cambrian strata intruded at depth by Jurassic and Cretaceous plutons. The 36 Ma Young Canyon pluton intrudes these same strata along the east flank of the range (Figs. 3–5). Incipient mylonitic fabrics associated with the southern Snake Range décollement are developed only along the easternmost flank of the range in the upper Precambrian to Cambrian Prospect Mountain Quartzite, Pioche Shale, and Pole Canyon Limestone. Geometrically similar ductile to brittle fabrics also involve the Young Canyon pluton (McGrew, 1993). Palinspastic restoration and analysis of balanced cross sections allowed McGrew (1993) to estimate that the southern Snake Range décollement and associated footwall mylonites accommodated between 8 and 18 km of total displacement in Tertiary time, during(?) and after the intrusion of the Young Canyon pluton. Any offset along younger, range-bounding faults is minor as only a thin (<1 km) accumulation of Tertiary sedimentary rocks is present in the valley between the southern Snake Range and Confusion Range (McGrew, 1993) (Fig. 4). K-Ar and $^{40}Ar/^{39}Ar$ total gas white mica ages from footwall rocks increase systematically westward, from Miocene (18–20 Ma) on the east side of the range to as old as 160 Ma on the west side (Fig. 3A) (Miller et al., 1988). The old ages on the west side reflect the main (Jurassic) metamorphic and intrusive event that affected this area, and indicate residence of rocks at temperatures cooler than about 350–400 °C since that time. The intermediate ages are presumably mostly partially reset ages that do not directly date cooling, but reflect partial argon loss during younger events.

We analyzed apatite from 9 samples of granitic rocks and 12 samples of low-grade metaquartzite from the footwall of the southern Snake Range décollement (Table 1 and Figs. 5–7). Virtually all granitic samples yielded high-quality data, whereas quartzite samples yielded only fair data and commonly had apatite yields that were too low to allow useful track length data to be collected. The results show a clear geographic distribution; samples from the eastern and central part of the range cluster tightly around 17 Ma in age and exhibit long mean track lengths with tight distributions. Plots of age versus east-west location for

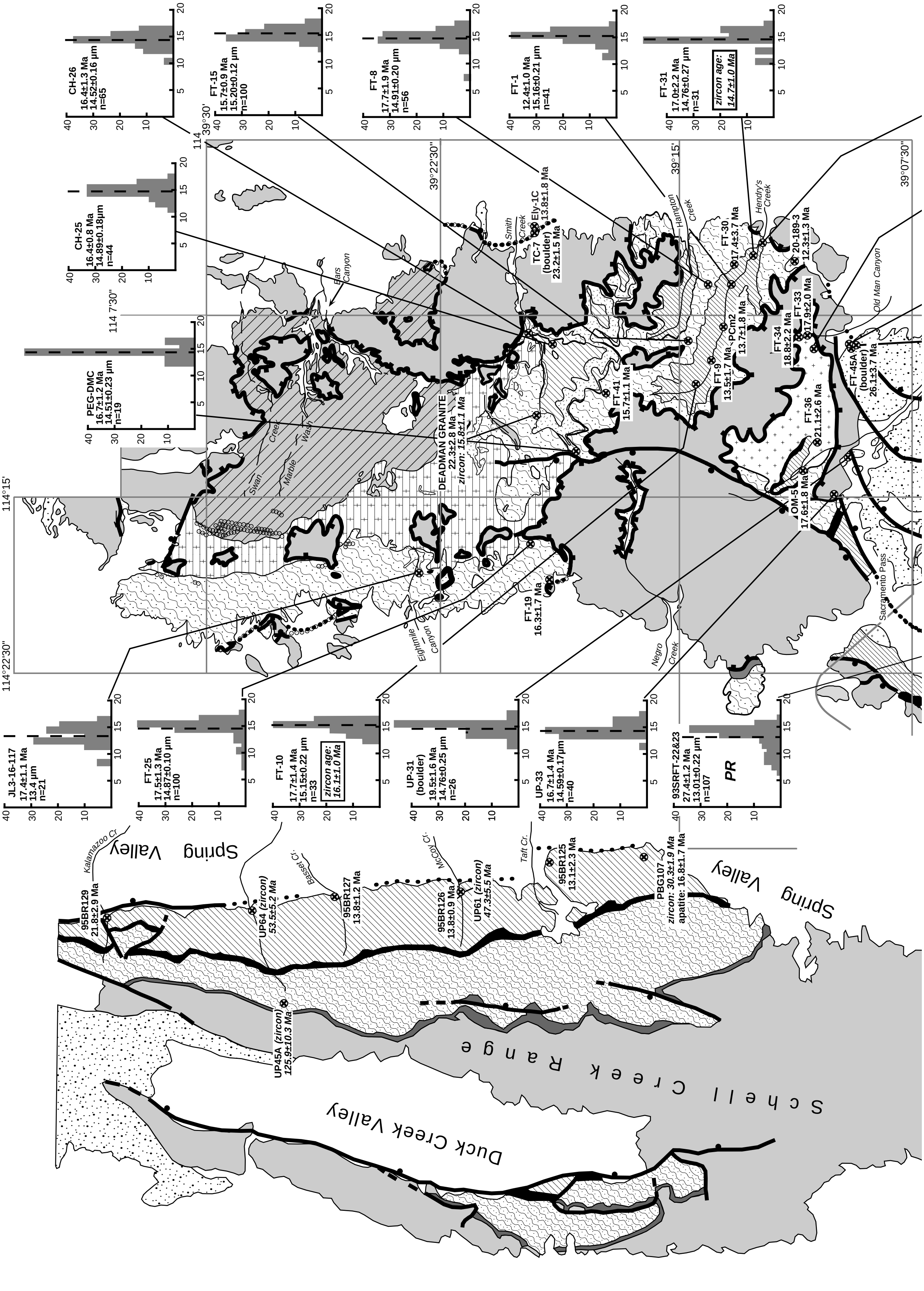
CH-26
16.4±1.3 Ma
14.52±0.16 µm
n=65
FT-15
15.7±0.9 Ma
15.20±0.12 µm
n=100
FT-8
17.7±1.9 Ma
14.91±0.20 µm
n=56
FT-1
12.4±1.0 Ma
15.16±0.21 µm
n=41
FT-31
17.0±2.2 Ma
14.76±0.27 µm
n=31
zircon age:
14.7±1.0 Ma
CH-25
16.4±0.8 Ma
14.89±0.18µm
n=44
PEG-DMC
16.7±1.2 Ma
14.51±0.23 µm
n=19
JL3-16-117
17.4±1.1 Ma
13.4 µm
n=21
FT-25
17.5±1.3 Ma
14.87±0.10 µm
n=100
FT-10
17.7±1.4 Ma
15.15±0.22 µm
n=33
zircon age:
16.1±1.0 Ma
UP-31
(boulder)
19.5±1.6 Ma
14.76±0.25 µm
n=26
UP-33
16.7±1.4 Ma
14.59±0.17µm
n=40
93SRFT-22&23
27.4±1.2 Ma
13.01±0.22 µm
n=107
PR
39°30'
114°
39°22'30"
39°15'
39°07'30"
114 7'30"
114°15'
114°22'30"
Bars Canyon
Smith Creek
Ely-1C
13.8±1.8 Ma
TC-7
(boulder)
23.2±1.5 Ma
Hampton Creek
Hendry's Creek
FT-30
17.4±3.7 Ma
20-189-3
12.3±1.3 Ma
Old Man Canyon
PCm2
13.7±1.8 Ma
FT-9
13.5±1.7 Ma
FT-34
18.8±2.2 Ma
FT-33
17.9±2.0 Ma
FT-41
15.7±1.1 Ma
FT-45A
(boulder)
26.1±3.7 Ma
FT-36
21.1±2.6 Ma
DEADMAN GRANITE
22.3±2.8 Ma
zircon: 15.8±1.1 Ma
Swan Creek
Marble Wash
OM-5
17.6±1.8 Ma
Sacramento Pass
FT-19
16.3±1.7 Ma
Eightmile Canyon
Negro Creek
Spring Valley
Kalamazoo Cr.
Basset Cr.
McCoy Cr.
Taft Cr.
95BR129
21.8±2.9 Ma
UP64 (zircon)
53.5±5.2 Ma
95BR127
13.8±1.2 Ma
95BR126
13.8±0.9 Ma
UP61 (zircon)
47.3±5.5 Ma
95BR125
13.1±2.3 Ma
PBG107
zircon: 30.3±1.9 Ma
apatite: 16.8±1.7 Ma
UP45A (zircon)
125.9±10.3 Ma
Schell Creek Range
Duck Creek Valley

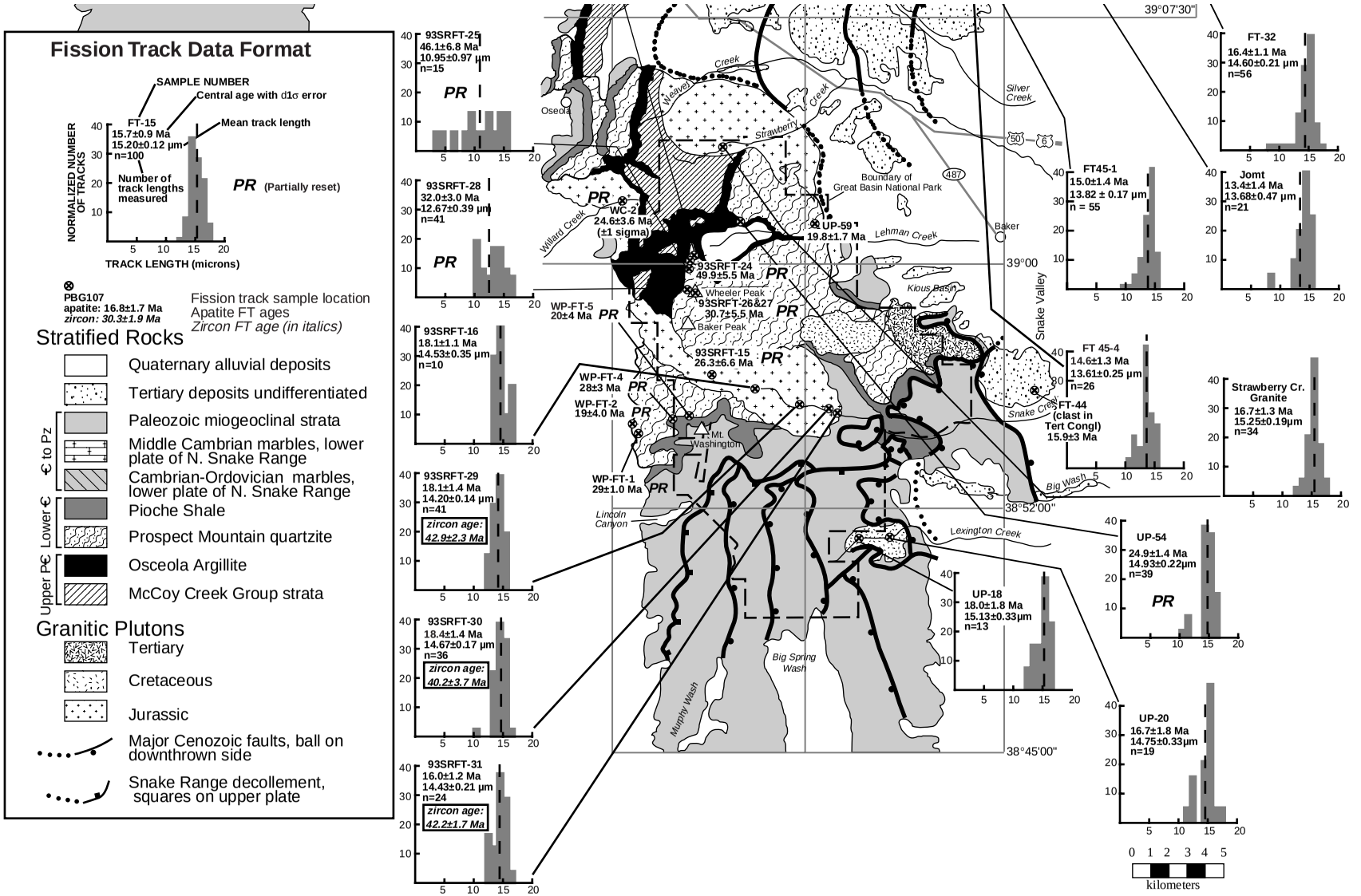

Figure 5. Expanded geologic map of the northern and southern Snake Range and part of the Schell Creek Range showing the location, ages, and track length data (where available) of fission-track samples. PR designates partially reset apatite ages on the western side of the southern Snake Range.

TABLE 1. FISSION TRACK SAMPLE LOCALITY, COUNTING, AND AGE DATA

Sample number	Irradiation number	Latitude (°N)	Longitude (°W)	Elevation (m)	No xls	Spontaneous Rho-S	Spontaneous NS	Induced Rho-I	Induced NI	$P(\chi^2)$ (%)	Dosimeter Rho-D	Dosimeter ND	Analyst	Age ± 1σ (Ma)
Northern Snake Range apatite samples														
20-189-3	LU012-03	39°11′20″	114°05′28″	1951	20	0.0714	95	1.2540	1667	27.0	1.2320	5792	ELM	12.3 ± 1.3
CH-25*	LU006-07	39°19′28″	114°08′28″	2024	20	0.2645	458	3.8480	6662	24.0	1.3600	5424	ELM	16.4 ± 0.8
CH-26*	LU005-08	39°19′42″	114°08′20″	1963	21	0.1668	292	2.3570	4126	2.9	1.3180	4356	ELM	16.4 ± 1.3
FT-1	LU011-05	39°13′34″	114°06′33″	2097	20	0.1858	152	3.4770	2845	94.0	1.3200	6052	ELM	12.4 ± 1.0
FT-8*	LU011-06	39°14′01″	114°06′13″	2472	20	0.0903	98	1.2020	1305	22.0	1.3420	6052	ELM	17.7 ± 1.9
FT-9	LU011-07	39°14′03″	114°09′01″	2316	20	0.0590	65	1.0490	1156	34.0	1.3650	6052	ELM	13.5 ± 1.7
FT-10*	LU011-08	39°14′24″	114°10′06″	2621	20	0.1144	186	1.5730	2558	14.0	1.3880	6052	ELM	17.7 ± 1.4
FT-15*	LU011-09	39°14′34″	114°08′12″	2871	20	0.5280	342	8.3190	5388	26.0	1.4110	6052	ELM	15.7 ± 0.9
FT-19WS	LU011-10	39°19′02″	114°18′33″	2073	21	0.1038	101	1.6020	1559	49.0	1.4330	6052	ELM	16.3 ± 1.7
FT-25WS*	LU011-11	39°19′22″	114°17′03″	2515	20	0.2924	329	4.2700	4804	1.4	1.4580	6052	ELM	17.5 ± 1.3
FT-30	LU024-11	39°13′12″	114°05′08″	2134	13	0.1067	80	1.3650	1023	0.0	1.2620	5616	ELM	17.4 ± 3.7
FT-31*	LU011-12	39°12′38″	114°04′47″	1811	20	0.1148	132	1.9510	2243	0.2	1.4800	6025	ELM	17.0 ± 2.2
FT-32*	LU006-05	39°12′26″	114°04′25″	1768	20	0.4359	231	6.0030	3181	53.0	1.2900	5424	ELM	16.4 ± 1.1
FT-33	LU024-12	39°11′37″	114°08′40″	2622	19	0.0926	87	1.1570	1087	66.0	1.2750	5616	ELM	17.9 ± 2.0
FT-34	LU024-13	39°11′28″	114°08′37″	2463	21	0.0945	79	1.1380	951	72.0	1.2900	5616	ELM	18.8 ± 2.2
FT-36	LU011-13	39°11′06″	114°13′10″	2579	21	0.0652	71	0.8145	887	32.0	1.5030	6052	ELM	21.1 ± 2.6
JL3-16-117	LU012-02	39°23′10″	114°18′20″	2250	25	0.1581	303	1.9440	3724	32.0	1.2150	5792	ELM	17.3 ± 1.1
Jomt	LU005-11	39°10′50″	114°08′21″	2256	22	0.0782	99	1.4140	1791	27.0	1.3750	4356	ELM	13.3 ± 1.4
OM-5	LU012-05	39°12′02″	114°14′55″	2377	20	0.0717	100	0.9089	1267	74.0	1.2700	5792	ELM	17.6 ± 1.8
PCM2	LU012-08	39°13′40″	114°07′32″	2200	15	0.1217	62	2.0540	1047	6.6	1.3250	5792	ELM	13.8 ± 1.8
PEG-DMC*	LU012-07	39°18′30″	114°13′00″	2169	19	0.1192	199	1.7160	2865	28.0	1.3700	5792	ELM	16.7 ± 1.2
UP-31 (clast)*	LU013-10	39°08′12″	114°14′30″	2000	22	0.0917	166	1.1560	2093	34.0	1.3990	5878	ELM	19.5 ± 1.6
UP-33*	LU013-11	39°09′15″	114°17′22″	2200	20	0.1757	158	2.6310	2366	11.0	1.4250	5878	ELM	16.7 ± 1.4
Deadman	LU032-05	39°17′16″	114°11′26″	2682	20	0.0684	72	1.4140	1488	46.0	2.6550	11988	RWB	22.3 ± 2.7
FT-41T	LU032-08	39°09′47″	114°10′08″	3158	20	0.5448	394	18.2400	13190	1.2	2.8850	11988	RWB	15.7 ± 1.1
FT-45A (clast)	LU032-09	39°07′50″	114°07′37″	1768	20	0.0936	55	1.8460	1085	71.0	2.9610	11988	RWB	26.1 ± 3.6
FT-45-1 (clast)	SU040-18	39°07′50″	114°07′37″	1768	18	0.0840	130	1.8040	2792	15.0	1.6580	4197	TAD	15.0 ± 1.4
FT-45-4 (clast)	SU040-19	39°07′50″	114°07′37″	1768	40	0.1037	147	2.2880	3243	8.6	1.6580	4197	TAD	14.6 ± 1.3
TC-7 (clast)	LU032-07	39°19′42″	114°03′50″	1689	20	0.3095	346	6.5000	7267	9.9	2.8080	11988	RWB	23.2 ± 1.5
Ely-1C (clast)	SU040-17	39°19′42″	114°03′50″	1689	16	0.0766	63	1.7610	1448	60.0	1.6280	4197	TAD	13.8 ± 1.8
Northern Snake Range zircon samples														
Deadman	LU068-09	39°17′16″	114°11′26″	2682	11	1.8750	457	2.9540	720	78.0	0.5667	2587	RWB	15.8 ± 1.0
FT-10	LU068-07	39°14′24″	114°10′06″	2621	14	1.0730	617	1.6480	947	28.0	0.5624	3130	RWB	16.1 ± 0.9
FT-31	LU068-08	39°12′38″	114°04′47″	1811	11	0.9349	475	1.5820	804	59.0	0.5674	2587	RWB	14.7 ± 0.9
Southern Snake Range apatite samples														
Strawberry*	LU012-13	39°03′32″	114°17′32″	2350	23	0.0982	189	1.4670	2823	12.0	1.4170	5792	ELM	16.6 ± 1.3
UP-18*	LU013-05	38°51′30″	114°13′13″	2500	23	0.1124	106	1.3820	1303	79.0	1.2620	5878	ELM	18.0 ± 1.8
UP-20*	LU013-06	38°51′40″	114°11′30″	2000	21	0.1345	133	1.8190	1799	4.5	1.2600	5878	ELM	16.7 ± 1.8
UP-54	LU014-01	39°01′34″	114°17′18″	3050	20	0.3813	355	3.2780	3052	7.2	1.2200	5626	ELM	24.9 ± 1.4
UP-59	LU014-02	39°01′10″	114°14′03″	2360	20	0.1656	149	1.8130	1632	20.0	1.2400	5626	ELM	19.9 ± 1.7
WC-2	LU012-09	39°01′59″	114°22′02″	2260	20	0.0318	52	0.3046	498	90.0	1.3430	5792	ELM	24.6 ± 3.6
FT-44 (clast)	LU032-02	38°55′28″	114°06′16″	1800	20	0.0740	100	1.9610	2651	73.0	2.4250	11988	RWB	15.9 ± 1.6
93SRFT-15	SU029-12	38°56′38″	114°18′01″	3389	10	0.2178	90	2.0890	863	0.4	1.7940	5079	TAD	26.3 ± 6.6
93SRFT-16*	SU029-14	38°56′26″	114°16′34″	2975	48	0.0810	332	1.5700	6438	20.0	1.8220	5079	TAD	18.1 ± 1.1
93SRFT-22/23	SU029-15	39°00′11″	114°19′07″	3231	43	0.4426	583	5.6650	7462	6.0	1.8220	5079	TAD	27.4 ± 1.2
93SRFT-24	SU029-16	39°00′03″	114°19′13″	3426	2	0.9397	95	6.6670	674	28.0	1.8410	5079	TAD	49.9 ± 5.5
93SRFT-25	SU029-17	38°59′52″	114°19′17″	3536	2	0.8519	53	6.5420	407	22.0	1.8410	5079	TAD	46.1 ± 6.8
93SRFT-26/27	SU029-18	38°59′10″	114°18′48″	3981	4	0.5734	34	6.6950	397	90.0	1.8590	5079	TAD	30.7 ± 5.5
93SRFT-28	SU029-19	38°59′17″	114°18′58″	3822	14	0.5764	246	6.3760	2721	4.9	1.8590	5079	TAD	32.0 ± 3.0
93SRFT-29*	SU029-20	38°55′47″	114°15′05″	2524	29	0.0710	170	1.4220	3405	34.0	1.8780	5079	TAD	18.1 ± 1.4
93SRFT-30*	SU029-21	38°55′27″	114°14′08″	2402	40	0.0794	251	1.5800	4992	0.8	1.8780	5079	TAD	18.4 ± 1.4
93SRFT-31*	SU029-22	38°55′22″	114°13′54″	2377	44	0.0654	198	1.4940	4525	47.0	1.8970	5079	TAD	16.0 ± 1.2
WPFT-1	SU034-04	38°55′03″	114°21′05″	2426	18	0.5566	474	6.0690	5168	56.0	1.6220	4808	TAD	28.6 ± 1.4
WPFT-2	SU034-05	38°55′20″	114°21′20″	2213	6	0.0686	24	1.1120	389	56.0	1.6220	4808	TAD	19.3 ± 4.1
WPFT-4	SU034-07	38°55′19″	114°19′35″	2773	14	0.3107	116	3.5230	1315	44.0	1.6430	4808	TAD	27.9 ± 2.7
WPFT-5	SU034-08	38°55′14″	114°18′55″	3042	6	0.2380	28	3.8260	450	15.0	1.6630	4808	TAD	19.9 ± 3.9
Southern Snake Range zircon samples														
93SRFT-29	SU039-13	38°55′47″	114°15′05″	2524	17	3.9950	1138	6.4210	1829	1.8	0.3065	4728	TAD	42.9 ± 2.3
93SRFT-30	SU039-17	38°55′27″	114°14′08″	2402	7	4.9900	941	8.5420	1611	0.0	0.3129	4728	TAD	40.2 ± 3.7
93SRFT-31	SU039-15	38°55′22″	114°13′54″	2377	12	4.0730	1172	6.6860	1924	8.5	0.3108	4728	TAD	42.2 ± 1.7
Schell Creek Range apatite samples														
PBG107B	LU012-11	39°15′42″	114°30′27″	1900	20	0.0675	69	0.9773	999	97.0	1.3800	5792	ELM	16.7 ± 2.1
95BR-125	SU028-19	39°19′38″	114°31′06″	2030	11	0.2821	34	7.3250	883	72.0	1.7610	4949	TAD	13.1 ± 2.3
95BR-126	SU028-20/21	39°22′30″	114°31′38″	2010	52	0.1725	255	4.2710	6315	5.2	1.7740	4949	TAD	13.8 ± 0.9
95BR-127	SU028-23	39°26′27″	114°32′12″	1980	17	0.2687	151	6.7150	3773	68.0	1.7860	4949	TAD	13.8 ± 1.2
95BR-129	SU028-25	39°33′49″	114°33′12″	1900	5	0.3529	59	5.6220	940	41.0	1.7990	4949	TAD	21.8 ± 2.9
Schell Creek Range zircon samples														
PBG107	LU025-08	39°15′42″	114°30′27″	1900	20	6.5180	2707	6.2550	2598	0.0	0.6428	1483	RWB	30.3 ± 1.9
UP-45A	LU025-07	39°28′20″	114°36′37″	2725	10	7.9290	906	1.6980	194	35.0	0.6207	2647	RWB	126. ± 10.0
UP-61	LU025-05	39°29′17″	114°30′32″	2000	10	5.8110	669	3.2570	375	0.1	0.5955	2647	RWB	47.3 ± 5.5
UP-64	LU025-06	39°22′30″	114°32′53″	2000	9	3.5740	333	1.7820	166	75.0	0.6113	2647	RWB	53.5 ± 5.2
Kern Mountains apatite sample														
SC†	LU005-03	39°38′32″	114°04′55″	2350	20	0.0699	105	0.8157	1226	66.0	1.2600	4356	ELM	18.9 ± 1.9

TABLE 1 (*CONTINUED*).

Notes: Abbreviations: No xls—number of individual crystals (grains) dated; Rho-S—spontaneous track density (x10^6 tracks per square centimeter); NS—number of spontaneous tracks counted; Rho-I—induced track density in external detector (muscovite) (x10^6 tracks per square centimeter); NI—number of induced tracks counted; P(χ^2)—χ^2 probability (Galbraith, 1981; Green, 1981); Rho-D—induced track density in external detector adjacent to dosimetry glass (x10^6 tracks per square centimeter); ND—number of tracks counted in determining Rho-D. Age is the sample fission track age; pooled age (Green, 1981) given when P(χ^2) > 5%, otherwise central age given (Galbraith and Laslett, 1993), calculated using zeta calibration method (Hurford and Green, 1983).

The following is a summary of key laboratory procedures. Samples analyzed by E. Miller and R. Brown were analyzed at La Trobe University; samples analyzed by T. Dumitru were analyzed at Stanford University. Apatites were etched for 20 s in 5N nitric acid at room temperature. Zircons were etched in eutectic NaOH:KOH melt at ~225 °C for 8–100 hr until well etched. Grains were dated by external detector method with muscovite detectors. Dosimetry glasses with external detectors were used as neutron flux monitors. Zeta calibration factors for specific minerals and dosimetry glasses were 351.25 (ELM apatite with glass SRM 612); 348 (RWB apatite with SRM 612); 389.5 (TAD apatite with glass CN5); 87.7 (RWB zircon with glass U3 for irradiation LU025); 88 (RWB zircon with U3 for irradiation LU068); and 447.3 (TAD zircon with CN5). Samples were irradiated in well-thermalized positions of Oregon State University (Stanford) or Lucas Heights reactor (La Trobe). External detectors were etched in 48% HF. At Stanford, tracks were counted with Zeiss Axioskop microscope with 100x air objective, 1.25× tube factor, 10× eyepieces, transmitted light with supplementary reflected light as needed; external detector prints were located with Kinetek automated scanning stage (Dumitru, 1993). At La Trobe, tracks were counted with Zeiss Universal microscope with 100× air objective, 1.25× or 1.6× tube factor, 10× eyepieces, transmitted light with supplementary reflected light as needed; external detector prints were located with Autoscan automated scanning stage (Smith and Leigh-Jones, 1985). Only grains with c-axes subparallel to slide plane were dated. Confined tracks lengths were measured only in apatite grains with c-axes subparallel to slide plane; only horizontal tracks measured (within ±~5°–10°), following protocols of Laslett et al. (1982). Lengths were measured with computer digitizing tablet and drawing tube, calibrated against stage micrometer (e.g., Dumitru, 1993). Data reduction was done with program by D. Coyle.

*Falls in totally reset cluster in Figure 6A; used in calculation of weighted mean age for range.

†Approximate locality.

these samples show no apparent systematic variation in age with distance from the eastern range front (Fig. 7B). In contrast, samples from the western flank of the range are distinctly older, ranging to 50 Ma, and exhibit broad, complex length distributions with many short tracks (these samples are designated PR in Fig. 5). We also analyzed zircon from three granitic samples. These samples, which are from a restricted area in the center of the range, yield concordant ages averaging 42 Ma.

The 17 Ma apatite samples were annealed at temperatures hotter than 110–125 °C before cooling rapidly at 17 Ma. This is indicated by their track length distributions and by the concordance of ages over a wide geographic area. The long track lengths require that the samples cooled rapidly to near surface temperatures (<50 °C) within several million years, indicating a minimum bound for the cooling rate of at least about 10–15 °C/m.y. (e.g., Green et al., 1989b). The older samples are inferred to have cooled at the same time, but from lower temperatures (and presumably less burial) where the fission-track clock was not completely reset to zero. This is evidenced by the systematic trend in these samples toward older ages and shorter mean track lengths (Fig. 6A), indicating that short, pre-17 Ma tracks are still present (e.g., Green et al., 1989a, 1989b; Dumitru, 1999).

In order to obtain the best possible estimate of the age of cooling in the southern Snake Range, and the uncertainty on that age, we calculated a weighted mean age and corresponding uncertainty from the ages of the seven southern Snake Range samples that are within the shaded 17 Ma cluster in Figure 6A (these samples are indicated in Table 1). These are the samples that exhibit track length distributions characteristic of rapid cooling from total annealing temperatures: the tight clustering and the fact that useful track length data could be collected indicate that they are generally the better quality samples. The resultant mean is 17.4 Ma with a 1σ uncertainty of 0.5 Ma (e.g., Dumitru, 1990, equations A2 and A3). This serves as the best estimate of the average time that the currently exposed rocks in the southern Snake Range cooled below 100 °C, the effective closure temperature of the apatite system in this situation. We also calculated mean ages for other areas (northern Snake Range apatites and zircons, Schell Creek Range apatites, and Kern Mountain apatites) that proved essentially concordant with 17 Ma (discussed in the following), as well as an overall weighted mean for all of the areas of 16.41 ± 0.25 Ma (±1σ).

On the basis of the reasoning discussed previously for calculating minimum amounts of fault slip based on apatite data (Fig. 2), at least 15 km of slip occurred along the southern Snake Range décollement in Miocene time; 12 km calculated from the horizontal distance across the range exposing 17 Ma samples, plus an inferred 3 km or more for the overlying partially annealed samples (Figs. 2, 5, 7, and 8). The fission-track data leave open the possibility of a somewhat greater amount of slip in Miocene time as well as the possibility of pre-Miocene slip on this fault. As for slip and exhumation since 17 Ma, the long track lengths in the 17 Ma samples indicate that they have resided at burial temperatures below 50 °C since soon after the 17 Ma cooling event. Therefore any late Miocene to recent exhumation has totaled no more than about 2 km. This inference is compatible with geologic data that suggest that any steeper faults bounding the east side of the southern Snake Range have limited displacement, based on the insignificant thickness of valley fill deposits between the southern Snake Range and the Confusion Range (Figs. 3 and 4).

Tertiary sedimentary sequences in the southern Snake Range support these conclusions and provide strong evidence for a two-stage history of motion along the southern Snake Range décollement (McGrew and Miller, 1995; Miller et al., in press). In the Murphy Wash region (Figs. 5 and 9), normal faults sole into the southern Snake Range décollement, and both hanging-wall faults and the tilted Paleozoic sequences they bound are unconformably overlain by a gently dipping conglomerate. This conglomerate is in turn overlain by a thin, unwelded crystal-rich rhyolite tuff dated as 31.07 ± 0.07 Ma and by a thick dacite ignimbrite dated as 30.29 ± 0.07 Ma (P. B. Gans, 1998, unpublished $^{40}Ar/^{39}Ar$ data). On the basis of its age, composition, and the presence of conspicuous large biotite phenocrysts, the dacite is correlated with the Cottonwood Wash Member of the Needles Range Group (Best et al., 1989). These relations provide compelling evidence for pre-31 Ma slip on this part of the fault system. In contrast, along the eastern flank of the southern Snake Range near Big Wash and Snake Creek (Figs. 5 and 9), tilted Tertiary fanglomerate sequences are as thick as 2 km and dip 40° to the west into the mapped continuation of the southern Snake Range décollement, which here dips 20° to the east (McGrew and Miller, 1995). These deposits commonly contain clasts of Needles Range volcanics, and so are younger than 31 Ma. The sequences also locally contain abundant clasts of footwall marble mylonite and granitic boulders derived from Jurassic granite currently exposed in the Snake Creek drainage. Apatite from one of these granitic clasts (sample FT-44) yields a fission-track age of 15.9 ± 1.6 Ma, concordant with ages from the nearby footwall rocks, and indicates a 16 Ma or younger age for these sedimentary rocks. Deposition in this basin was coupled to slip along the currently low-angle fault bounding the western side of the basin; we previously mapped this fault as the southern Snake Range décollement. We now realize that this particular fault (labeled 2 in Fig. 4D) must be younger, and perhaps cuts the older portion of the southern Snake Range décollement mapped farther west and south in the range. In map view and cross section,

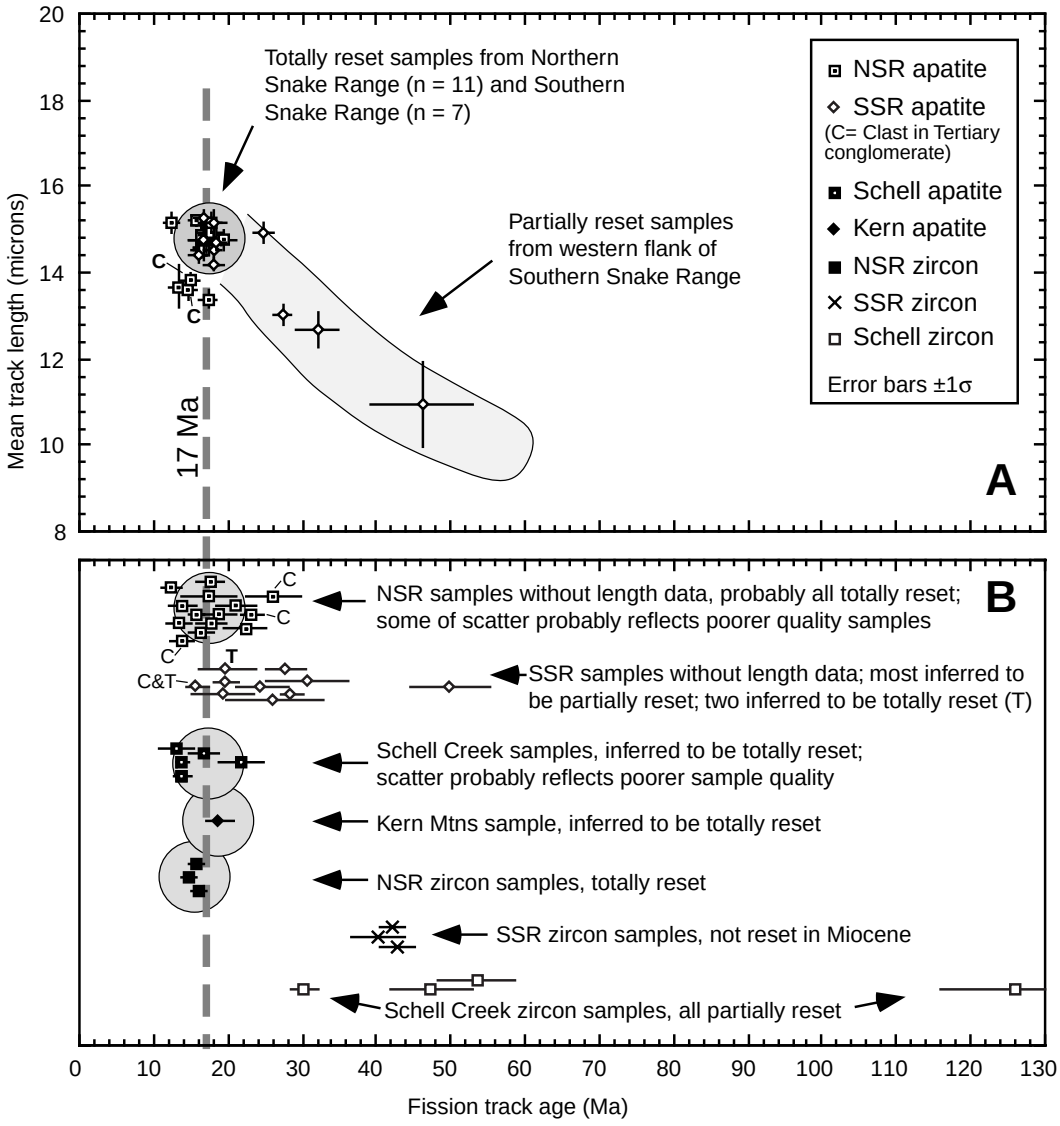

Figure 6. (A) Plot of apatite fission-track age vs. mean track length for northern and southern Snake Range (NSR, SSR) samples for which track length data could be collected. Apatite samples that cool rapidly from hotter than 125–100 °C (total annealing temperatures) to cooler than 50 °C should exhibit long mean track lengths of 14–15.5 μm (Gleadow et al., 1986; Green et al., 1989a, 1989b). Note pronounced clustering of samples with such lengths around an age of 17 Ma, indicating major cooling at that time. Samples from the western flank of the southern Snake Range exhibit systematically older ages and shorter mean track lengths, interpreted to indicate cooling at 17 Ma but from starting temperatures insufficient to fully anneal tracks (cooler than 100–125 °C) (cf. Green, 1989). This is evidence of lesser unroofing in this area. (B) Plot of apatite fission-track ages for samples for which track length data could not be collected due to, e.g., low track numbers and low apatite yields. Plot also includes zircon fission-track ages. All of these samples are inferred to be totally annealed and to directly date cooling, except for some of the southern Snake Range apatite samples, possibly the southern Snake Range zircon samples, possibly a few of the northern Snake Range samples, and all of the Schell Creek Range zircon samples. Total annealing is inferred because of the consistency of ages, the fact that nearby samples exhibit 14–15.5 μm mean lengths (northern and southern Snake Range), and the concordance of zircon and apatite ages (northern Snake Range). Older apatite ages from western flank of southern Snake Range reflect cooling at 17 Ma from temperatures insufficient to fully anneal tracks (<125 °C). Gans et al. (1991) reported apatite and zircon fission-track data and biotite $^{40}Ar/^{39}Ar$ ages from the Deep Creek Range and interpreted them to indicate extended cooling over about the period 18–14 Ma, overlapping with the strong 17 Ma age cluster shown here.

the two faults merge into one another, so that documenting their crosscutting relations was impossible without data on the relative timing of fault slip. In summary, the information discussed here indicates two periods of motion on the southern Snake Range décollement, (1) pre-31 Ma motion in its western reaches, and (2) Miocene motion, ongoing at 17 Ma, along the entire eastern flank of the range. Miocene slip, estimated to be at least 15 km, thus accounts for most of the 8–18 km of total slip estimated by McGrew (1993) for the southern Snake Range décollement.

Three zircon samples from a restricted area in the center of the range yielded concordant ages (Figs. 5 and 6B) with a weighted mean age of

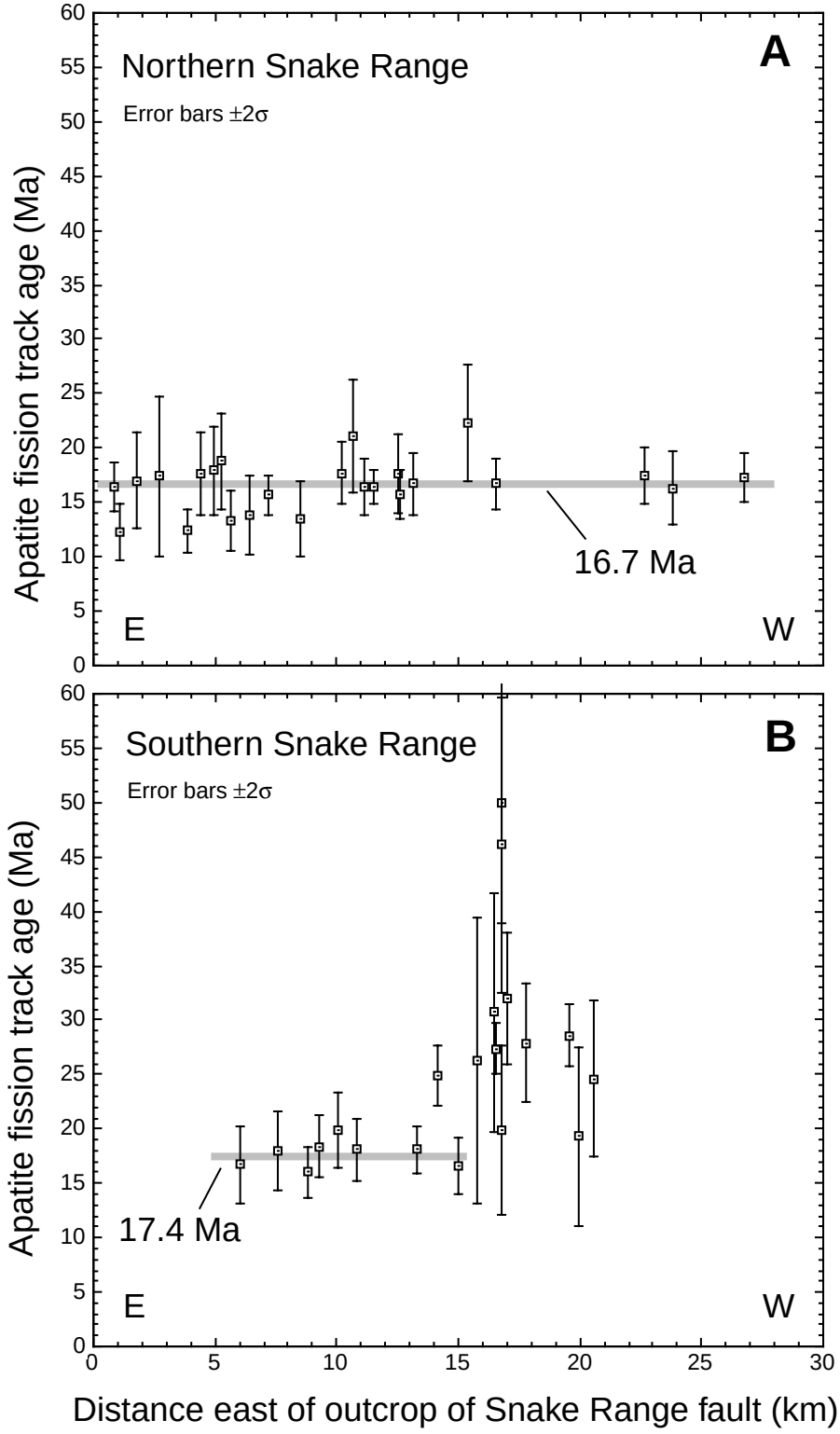

Figure 7. Plot of apatite fission-track ages vs. distance from the easternmost flank of the southern and northern Snake Range. In the northern Snake Range (A), ages are essentially invariant across the entire width of the range and indicate major cooling at 17 Ma. In the southern Snake Range (B), apatite ages are invariant across the entire width of the range and also indicate major cooling at 17 Ma. Samples with older ages along the western margin of the range were at shallower depths where fission-track annealing was only partial before cooling at 17 Ma. Much of the age-scatter exhibited by these older samples correlates with sample elevation and derives from the fact that higher elevation samples were at shallower burial depths and thus lower burial temperatures before cooling at 17 Ma.

42.2 ± 1.3 Ma. These ages may indicate major cooling at that time, in which case they may reflect some of the pre-29–31 Ma faulting in the range. Alternatively, these may be mixed ages that do not directly date a specific cooling event. In either case, these ages, in conjunction with the apatite data, indicate that before the start of the 17 Ma cooling event, samples in the center of the range resided at crustal temperatures somewhere between about 125 and 300 °C. The samples with older apatite ages on the west flank of the range resided at temperatures <110–125 °C before the start of the 17 Ma exhumation event, and the 18–20 Ma white mica argon ages along the easternmost flank of the range (Fig. 3A) indicate temperatures hotter than about 350 °C before exhumation. Together, these data indicate asymmetric Miocene exhumation of the range, with much greater exhumation on the east, and suggest that the tilted fault-block model of Figure 2 is likely applicable to the southern Snake Range.

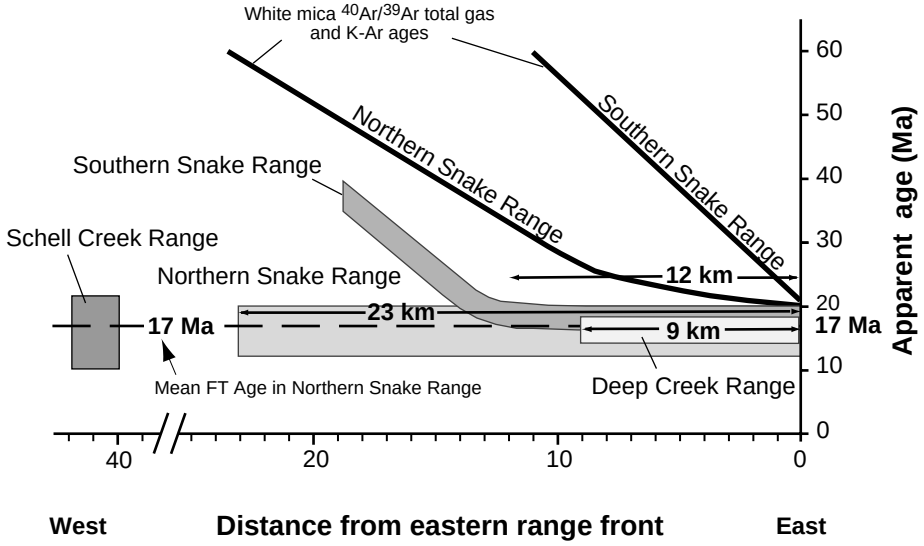

Figure 8. Schematic plot of fission-track (FT) ages with respect to distance as measured from the eastern flanks of the ranges. All data are from this paper, except the Deep Creek Mountains data, which are summarized from Gans et al. (1991). As per the model of Figure 2, minimum estimates of the amount of Miocene slip (and the minimum horizontal extension) are given by summing the horizontal distances measured between samples that yield concordant ages and long track length distributions with the inferred conservative 3 km thickness estimate for the overlying partial annealing zone. The distances exhibiting concordant ages are indicated for each range in question.

Northern Snake Range

The well-developed footwall mylonites of the northern Snake Range stand in contrast to the general lack of such fabrics in the southern Snake Range. The severe thinning of stratigraphic units in the footwall of the northern Snake Range versus the southern Snake Range (Fig. 4) is the consequence of this strain. The thick section of Tertiary strata exposed between the two ranges in the Sacramento Pass area obscures the exact reason for this abrupt northward strain gradient. These differences in strain are coupled with differences in the Miocene thermal history of the two parts of the Snake Range (discussed in the following) and together may be key reasons for the localization and preservation of the Sacramento Pass sedimentary basin.

Map units in the footwall of the northern Snake Range décollement are everywhere gently dipping and parallel to the overlying low-angle detachment fault (Figs. 4 and 5). All units are severely thinned and are stretched in a N60W direction, the result of strain associated with the development of mylonitic fabrics (Miller et al., 1983; Lee et al., 1987; Lee and Sutter, 1991). The 10°–20° dipping fault system exposed along the east side of the range and the parallel footwall fabrics can be followed in the subsurface on seismic reflection data. These reflectors are not offset by any significant faults between the Snake and Confusion Ranges (Gans and Miller, 1985). Strain associated with mylonitic fabrics systematically decreases westward in the range and eventually dies out along the very northwestern edge of the range (Fig. 3A) (Lee et al., 1987; Lee and Sutter, 1991). The fabrics and associated strain are inferred to continue with depth in the crust where they developed at higher temperatures (Lee et al., 1987). Thus, footwall rocks underwent penetrative deformation and wholesale change in shape as detachment faulting and exhumation took place. For these reasons, it is likely that the northern Snake Range does not represent a rigid tilted fault block, compromising the direct utility of the fission-track approach illustrated in Figure 2.

Mylonitic fabrics overprint Late Cretaceous intrusive and metamorphic rocks on the northwest flank of the range. Muscovite from an undeformed rhyolite porphyry dike that cuts mylonitic fabrics yielded a plateau age of 36.9 ± 0.3 Ma, whereas compositionally similar (but undated) dikes to the east are involved in the mylonitic deformation, suggesting a two-stage history for mylonite development (Lee and Sutter, 1991; Lee et al., 1987). Contours of K-Ar and total gas $^{40}Ar/^{39}Ar$ ages mimic the strain gradient within the footwall rocks with a systematic decrease eastward from a high of 60 Ma to a low of 20 Ma (Fig. 3A). This pattern is similar to that observed in the southern Snake Range, but all ages are younger and the "chrontours" are more widely spaced. Based on the prevalence of disturbed $^{40}Ar/^{39}Ar$ spectra, Lee and Sutter (1991) reasoned that the gradient in ages did not indicate progressive cooling, but rather was the result of both cooling and one or more reheating events with attendant partial argon loss. They concluded, however, that the rocks along the eastern side of the range resided at higher temperatures for longer periods of time, and that this relationship was compatible with asymmetric unroofing of the range. Lee (1995), utilizing multiple diffusion domain analysis of $^{40}Ar/^{39}Ar$ data from K-feldspars, showed that rocks along the eastern side of the range resided at temperatures above 300 °C throughout Oligocene time, until about 20 Ma. In contrast, the western side of the range had already cooled below 300 °C by 46 Ma. These data indicated differential cooling (earlier on the west) and suggested at least two, and perhaps three, episodes of rapid cooling related to slip on the overlying detachment fault. Based on the modeling of the K-feldspar data, supplemented by our preliminary apatite fission-track data, these episodes were thought to be middle Eocene (48–41 Ma), late Oligocene (30–26 Ma), and early Miocene (20–16 Ma) age (Lee, 1995). However, footwall rocks across the entire eastern half of the range, from the range crest to its eastern flank, apparently resided at temperatures above 300 °C until the youngest event. The fission-track data indicate exhumation of footwall rocks in Miocene time, ca. 17 Ma. Lee (1995) argued that all mylonitization was likely over by 20 Ma, but the combined zircon and apatite fission-track data (discussed in the following) leave open the possibility that mylonitic fabrics along the eastern side of the range could be slightly younger, perhaps as young as 17 Ma.

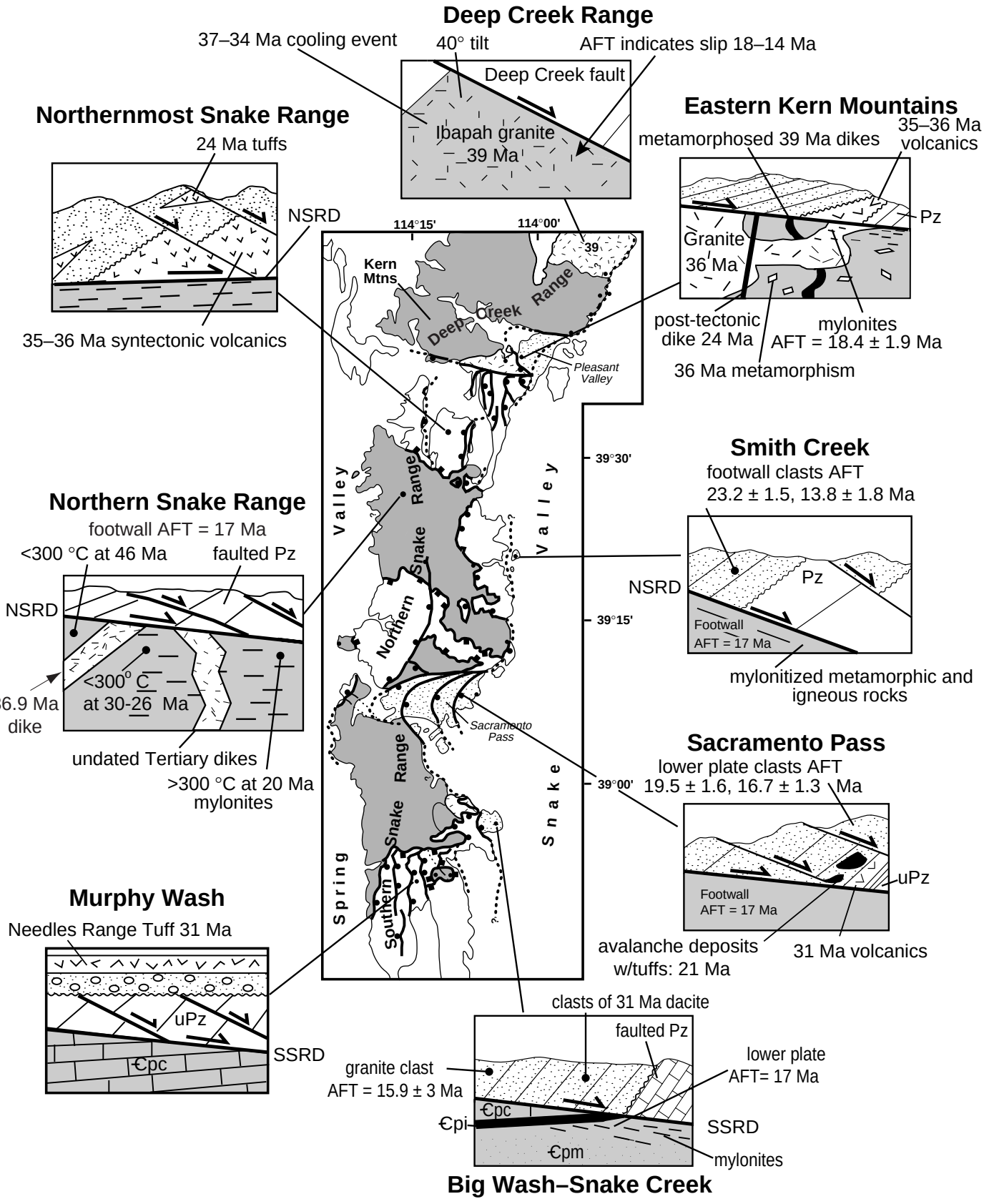

Figure 9. Summary of available timing constraints on the age of faulting emphasizing the evidence for two distinct episodes of motion on the Snake Range–Deep Creek Range fault system. See text for detailed discussion. NSRD—northern Snake Range décollement; SSRD—southern Snake Range décollement; AFT—apatite fission-track age.

We analyzed 22 apatite and 3 zircon samples from the footwall of the northern Snake Range (Table 1). All metamorphic and plutonic rocks yielded abundant apatite, generally of good to excellent quality. Many of the metamorphic rocks yielded particularly high quality apatite, which grew during Cretaceous amphibolite facies metamorphism and which is still coarse grained despite severe grain-size reduction of the enclosing rocks during mylonitization.

Of the 14 apatite samples with track length data, 11 cluster tightly around an age of about 17 Ma and a mean track length of 14–15.5 mm, and the remaining three plot only slightly outside of this cluster (Fig. 7A). The remaining samples without length data also generally cluster around a 17 Ma age (Fig. 7B). The weighted mean age of the 11 well-clustered samples in Figure 7A probably provides the best estimate of the mean time of cooling below about 100 °C, yielding an age of 16.7 ± 0.4 Ma (±1σ), whereas all 14 samples with length data yield an age of 16.2 ± 0.3 Ma. Plots of age versus east-west location show no apparent systematic variation in age across the entire east-west extent of the footwall exposure (Figs. 6 and 7). In addition, the three zircon samples yielded ages of 14.7 ± 1.0, 16.1 ± 1.0, and 15.8 ± 1.1 Ma (±1σ) with a weighted mean of 15.5 ± 0.6 Ma, concordant within 2σ uncertainty with the mean 16.7 ± 0.4 Ma apatite age. These data indicate that rocks in the footwall of the northern Snake Range cooled very rapidly from hotter than 310 °C, the total annealing temperature of zircon (see Tagami and Dumitru, 1996), to cooler than 50 °C, implying a minimum cooling rate of at least 100 °C/m.y. These data place a younger age limit on the formation of footwall mylonites, which are believed to develop by crystal plastic flow in quartzose rocks at temperatures between about 300 and 450 °C (e.g., Koch et al., 1989; Tullis, 1990).

In summary, the fission-track data indicate Miocene exhumation of the entire east-west extent of the central part of the northern Snake Range, a distance of about 23 km (Fig. 3, 7, and 8). However, several lines of reasoning argue that the exposures of the Snake Range décollement in the western part of the range may have ceased moving by Miocene time. Minerals with higher blocking temperatures indicate exhumation by faulting in the northwest part of the range in late Eocene–early Oligocene time or earlier (Lee, 1995). The décollement is bent, folded, or domed so that it now dips west in this region. This event precluded continued eastward slip along this portion of the décollement. The bend is partially the result of reverse drag of units into the adjacent Schell Creek fault to the west (Figs. 4 and 6) (Gans and Miller, 1985), but is also related to uplift of the northern Snake Range relative to flanking valleys. Along strike of this bend to the south, a single, down-to-the-west normal fault has been mapped, the displacement of which increases southward. This fault apparently also served to accommodate uplift of the crest of the range relative to its western flank (Figs. 3, 4, and 5). These structures in combination could be viewed as the result of isostatically driven vertical uplift and associated doming of the northern Snake Range. If so, our fission-track ages from this side of the range may date this uplift, but not necessarily the age of slip along the western part of the northern Snake Range décollement. Available fission-track data from the Schell Creek Range are much more limited than in the northern Snake Range, and the quality of the dated apatites (mostly from low-grade metaquartzites) is quite poor. However, four samples from the base of the Schell Creek fault block, which is tilted about 30°–40° to the west (Gans et al., 1985), yield apatite ages with a weighted mean of 14.8 ± 0.6 Ma. Considering the poor sample quality, this age is essentially concordant with the ages from the Snake Range. These ages are compatible with the interpretation that major slip on the Schell Creek fault occurred during uplift and arching or doming of the northwestern Snake Range and during slip along the eastern part of the northern Snake Range décollement (eastern side of the range). In other words, the exhumation and cooling recorded by samples from the northern Snake Range was coeval with high-angle rotational faulting along the major range-bounding fault of the Schell Creek Range. The rugged geomorphology of the Schell Creek Range and evidence for recent motion on the range-bounding fault based on scarps in alluvium indicate that some of the motion along this fault is younger than Miocene age. The fission-track data place an upper bound of about 4 km on this post-Miocene slip (assuming a low thermal gradient of 20–25 °C/km); otherwise younger fission-track ages would be observed.

Zircon fission-track ages from the Schell Creek Range structural block are much older and more variable than those from equivalent stratigraphic units in the northern Snake Range (Figs. 5 and 6). This indicates that the crustal levels exposed in the Schell Creek Range were at temperatures between 125 and 300 °C in Miocene time (resulting in incomplete resetting of zircon ages), and thus that these units underwent significantly lower temperatures in Miocene time than did equivalent stratigraphic units in the northern Snake Range (Figs. 4 and 5). The total amount of slip on the Schell Creek fault is calculated from map relations to be about 10–12 km, all of which probably postdates motion on the northwesternmost portion of the Snake Range décollement, which it cuts (Gans et al., 1985). Based on our data alone, it is unclear if most of that slip is Miocene age, occurring ca. 17 Ma, or perhaps older. In any case, Miocene temperatures in the crust were considerably lower here than in the northern Snake Range.

Tertiary sedimentary and volcanic rocks flank the northern Snake Range and are best exposed in the Sacramento Pass and Kern Mountains transverse zones (Fig. 3). These sequences shed additional light on the timing of faulting in the Snake Range and provide supporting evidence for the two-stage history of fault motion outlined from the thermochronologic data.

The Tertiary section in Sacramento Pass is about 2 km thick, generally dips about 30°–40° to the west, and was deposited unconformably over Paleozoic strata (Grier, 1983, 1984; Miller and Grier, 1995). The Tertiary section and underlying rocks are now fault bounded on all sides of their present outcrop area and are cut and repeated by several subparallel, arcuate normal faults that merge with the main range-bounding faults to the north and south (Figs. 3 and 5). The oldest deposits of the basin include volcanic rocks, lacustrine limestone, marl, and lesser conglomerate (Fig. 9). An age of 35 Ma was preferred for the volcanic rocks at the base of the succession (see review in Gans et al., 1989), but Martinez et al. (1998) reported a new $^{40}Ar/^{39}Ar$ biotite age of 31 Ma for these volcanic rocks. Large lenses of intensely brecciated Paleozoic strata, interpreted as rock-avalanche deposits likely derived from a region of steep topography, occur within this older succession (Grier, 1984; Miller et al., 1996; Martinez et al., 1998). Based on their map geometry, the avalanche deposits were derived mostly from the west or southwest margin of the basin. A 21.0 ± 0.5 Ma $^{40}Ar/^{39}Ar$ biotite age on underlying tuffaceous horizons indicates an entirely Miocene age for the avalanche deposits (Martinez et al., 1998).

The upper part of the Sacramento Pass sedimentary sequence consists of coarse alluvial-fan deposits derived mainly from the southwest, based on paleocurrent analyses and the presence of clasts of distinctive granite and metasedimentary rocks common only to the northernmost part of the southern Snake Range (Miller et al., 1996). One of these granite boulders yielded an apatite fission-track age of 19.5 ± 1.6 Ma (sample UP-31), concordant within ±2σ with ages from footwall granitic rocks of the southern Snake Range and compatible with the inference of an episode of rapid Miocene exhumation and erosion. Conglomerates in a more easterly fault block (sample locality FT-45A, Fig. 5) contain clasts of mylonitic two-mica granite derived from the Jurassic Silver Creek granite exposed exclusively in the upper Silver Creek drainage in the northern Snake Range (Fig. 5). Palinspastic restorations indicate that this easterly fault block restores to the position of the Silver Creek drainage (Miller and

Grier, 1995), and thus the northern Snake Range also served as a source area for at least part of the younger fanglomerates in the sequence. Three clasts from sample locality FT-45 yielded apatite ages of 26.1 ± 3.7, 15.0 ± 1.4, and 14.6 ± 1.3 Ma. The younger two ages are concordant with the apatite exhumation ages from the footwall samples in the northern Snake Range. The older age could be spurious or the dated clast could be from a source area or structural level where apatites were not fully annealed before the 17 Ma cooling event. The preservation of such levels is not apparent from the fission-track data on samples from the present footwall exposures of the northern Snake Range, but these levels may have been removed by relatively minor erosion between Miocene time and today.

The new geochronologic data reported by Martinez et al. (1998) suggest that most of the Sacramento Pass sedimentary succession is Miocene age or younger, because the base of the section that includes the rock- avalanche deposits is dated by a tuff as 21 ± 0.5 Ma. These deposits thus herald a major period of uplift, erosion, and exhumation in Miocene time, compatible with fission-track data from the footwall units. The faults that cut the Sacramento Pass section merge into the main trace of both the northern and southern Snake Range décollement, thus dating motion along the eastern part of what has been mapped as the Snake Range décollement as Miocene age or younger. Palinspastic restoration indicates that this group of faults represents a minimum of 5 km of horizontal extension (Miller et al., 1996).

Tertiary deposits are locally exposed along the northeastern side of the northern Snake Range. At the mouth of Smith Creek (Fig. 5), relations similar to those in Sacramento Pass are evident. Here, a sequence of Tertiary conglomerates is tilted 40° to the west and is bound beneath by a low-angle fault that dips 15°–20° to the east. This sequence includes clasts of mylonitic footwall rocks that can be matched to distinctive bedrock units exposed in the upper part of the Smith Creek drainage (Gans et al., 1999a). As the low-angle fault cuts sedimentary units hosting clasts of footwall lithologies, it must also cut the northern Snake Range décollement as mapped higher in the range (cf. faults labeled 1 and 2 in Fig. 4C). Two of these clasts of mylonitic rock (TC-7 and Ely-1C) yielded apatite fission-track ages of 23.2 ± 1.5 and 13.8 ± 1.8 Ma. The younger age is concordant with the ages from the footwall samples in the northern Snake Range, whereas the older age could be spurious or derived from a structural level where apatites were not fully annealed before the 17 Ma cooling event.

The Snake Range décollement is inferred to be at a shallow depth (<1 km) beneath the region between the northern Snake Range and the Kern Mountains (Fig. 4B) (Gans et al., 1989). Here, the early Oligocene Kalamazoo volcanic and associated shallow intrusive rocks constitute the bulk of the Tertiary succession in the hanging wall of the décollement. Poorly exposed, younger sedimentary rocks were deposited across the dominantly volcanic succession. The entire sequence is faulted and tilted westward, with dips decreasing from 35° to 10° upsection. Part of the fault-related tilting was coeval with Kalamazoo volcanism at about 35 Ma, and these faults sole into the northern Snake Range décollement in the shallow subsurface (Gans et al., 1989) (Fig. 9), indicating an earliest Oligocene episode of motion along the décollement. The volcanic rocks are overlain by more gently dipping conglomerate and lacustrine sedimentary rocks. A vitric tuff dated as 24 Ma is interstratified with these sedimentary rocks, placing an upper age limit on the older episode of normal faulting and suggesting that the faults that cut the entire sequence continued to move after earliest Miocene time (Gans et al., 1989). Coarse, very gently dipping conglomerates cap the sequence and contain granitic and metamorphic rocks derived from footwall rocks in the nearby Kern Mountains. The stratigraphy and age constraints from this sequence suggest faulting in earliest Oligocene time (35 Ma) and also after 24 Ma, compatible with the history of footwall uplift deduced from thermochronologic data in the northern Snake Range and compatible with the one 18.4 ± 1.9 Ma fission-track apatite age from the adjacent Kern Mountains portion of the footwall (discussed in the following).

Kern Mountains and Deep Creek Range

The Kern Mountains and Deep Creek Range are underlain by a 13–14-km-thick upper Precambrian to Paleozoic shelf sequence intruded by the Late Cretaceous (75 Ma) Tungstonia Granite and the Eocene-Oligocene Skinner Canyon (35 ± 1 Ma) and Ibapah (39 Ma) granites (Miller et al., 1988; Rodgers, 1987; Gans et al., 1990, 1991). Post-Eocene tilting of the two ranges by 35°–45° is indicated by the dips of the Paleozoic succession and overlying latest Eocene volcanic rocks (Gans et al., 1990, 1991). The separation or offset of Tertiary volcanic rocks present in both footwall and hanging wall indicates ~15 km of cumulative slip along the range-bounding fault in the Deep Creek Range and to 25 km of total separation along the fault system that unroofed the Kern Mountains (Rodgers, 1987; Gans et al., 1991). Along the Kern Mountains segment of the fault, part of this separation accumulated due to nonrigid footwall behavior and intrusion of the Skinner Canyon granite.

Mylonitic fabrics are developed only along the easternmost tip of the Kern Mountains and involve Paleozoic strata that were metamorphosed and deformed during intrusion of the Skinner Canyon granite (Gans et al., 1990; Miller et al., 1994a). The fabrics also involve the border phases (dikes and sills) of the granite, but the main phase of the pluton is undeformed. A transect of seven apatite samples from the larger Cretaceous Tungstonia Granite that underlies the Kern Mountains proved undatable because the apatites are full of tiny zircon inclusions (as noted by Best et al., 1974). The only sample that contained datable apatite was collected from the Skinner Canyon granite and yielded a fission-track age of 18.4 ± 1.9 Ma, concordant with ages from the northern Snake Range (Figs. 3A, 7, and 9).

In the Deep Creek Range, a detailed study by Gans et al. (1991) utilized apatite and zircon fission-track dating in conjunction with $^{40}Ar/^{39}Ar$ dating of muscovite, biotite, and K-feldspar to determine the age of exhumation and cooling related to tilting and block rotation of the Deep Creek Range. Two discrete ages of fault slip and tilting are indicated, one in Oligocene time (37–34 Ma) and another in Miocene time (18–14 Ma). The data suggest that the Miocene event lasted several million years with the best estimate for the period of major slip being from about 18 to 14 Ma. Part of the total slip on the Deep Creek–Kern Mountains part of the fault system likely accumulated in Eocene-Oligocene time, coeval with intrusion of the Skinner Canyon granite. Based on the apatite fission-track data set from the Deep Creek Mountains, however, a very minimum of 12 km of slip must have accumulated during the Miocene event (Gans et al., 1991) (Fig. 8).

Summary

In summary, the sedimentary and volcanic sequences that now constitute part of the hanging wall of the Snake Range–Deep Creek Range fault system support a two-stage movement history, as do the thermochronologic data from footwall rocks (Fig. 9). The thermochronologic data provide compelling evidence for a major episode of Miocene slip along this fault system, the Deep Creek data indicating slip over the period 18– 4 Ma and the northern and southern Snake Range data indicating major slip at 17 Ma (Fig. 9). Absolute age constraints on the early Oligocene event are based mostly on stratigraphic data, the age of volcanic rocks, and the cooling history of minerals with higher blocking temperatures. These data indicate a late Eocene–early Oligocene age, as previously suggested (e.g., Gans and Miller, 1983; Gans et al., 1989). The new fission-track database provides a reasonable estimate of how much of the

total extensional strain is represented by the younger of the two events. The combined fission-track data along the entire length of the fault system suggest a minimum of 12–15 km of dip-slip motion along the entire fault system in Miocene time (Fig. 8), with likely greater horizontal extension represented by the central part of the fault system in the northern Snake Range.

DISCUSSION AND CONCLUSIONS

The fission-track data from east-central Nevada provide useful constraints on the time of faulting and exhumation that led to the development of the Deep Creek Range, Schell Creek Range, and the northern and southern Snake Range. Prior to the acquisition of these new data, crosscutting relations and volcanic stratigraphy indicated that extension at the regional scale had begun during latest Eocene to early Oligocene time and was closely tied to magmatism (e.g., Gans et al., 1989). Although geologic relations indicated that extension continued after this time, few bracketing relations existed to document the ages and the magnitudes of the younger events. Because younger extension was so poorly dated, we seriously underestimated its significance in our earlier publications on the geology of the region.

The evidence summarized in this paper demonstrates that a major period of rapid extension occurred across the region during Miocene time, ca. 17 Ma. During a few million years, a minimum of 12–15 km of slip and a comparable or greater amount of horizontal extension occurred along the main fault system that bounds the eastern side of the Deep Creek Range and northern and southern Snake Range.

An important aspect of the data set is that it indicates that movement along the low-angle Snake Range décollement in the northern Snake Range was contemporaneous with normal slip on high-angle faults along strike in the southern Snake Range to the south and the Kern Mountains and Deep Creek Range to the north. Thus it appears that the development of low-angle metamorphic core complex detachment faults can occur together in space and time with more typical Basin and Range–style, high-angle, rotational faults. In the following discussion we explore the implications of our database for the evolution of the Snake Range metamorphic core complex and address a more speculative question. Do detachment faults like the Snake Range décollement represent evolutionary end-members of high-angle rotational faults or do they represent distinctly different phenomena?

Early in the history of thought on how core complexes develop, Davis (1983) suggested that detachment faults might represent examples of rotated high-angle normal faults with large amounts of total slip, eventually exhuming mylonites formed at depth in the Earth's crust. The lack of apparent tilting of the footwall of the northern Snake Range over more than 25 km in the direction of motion of the overlying fault, the inference that ductile flow of lower plate rocks was pervasive and continued to greater depths beneath the detachment, and the complexity and extreme amount of extension represented by the mosaic of upper plate normal faults, are all important characteristics of the Snake Range that do not easily fit such a model. These characteristics led us to propose more of a "pure-shear stretching" or "ductile-brittle transition zone" model for the northern Snake Range décollement (e.g., Miller et al., 1983; Gans et al., 1985; Lee et al., 1987). The interpretation that core complex detachment faults represent large-displacement, very low angle faults (Wernicke, 1985) was an influential model for structures like the Snake Range décollement, but the characteristics described above were also difficult to incorporate into this model (e.g., Gans and Miller, 1985). Furthermore, low-angle fault models have been criticized because it is mechanically difficult for these to move in the Earth's crust and because there have been few or no earthquakes documented on low-angle faults in actively extending regions (e.g., Jackson and McKenzie, 1983; Jackson and White, 1989; see Wernicke, 1995). These criticisms led to a rather different but mechanically more satisfactory explanation for low-angle faults termed the "rolling-hinge" model (Buck, 1988; Wernicke and Axen, 1988; Hamilton, 1988; Wdowinski and Axen, 1992). The rolling hinge model attempts to combine observational data on very low-angle extensional faults while honoring rock mechanical principles, explaining areally extensive low-angle detachment faults as the result of progressive development and rotation of steeply dipping faults that bound the migrating edge of a low-strength footwall, which deforms easily and rapidly as a consequence of tectonic unloading. Lee (1995) analyzed the cooling histories of rocks in the Snake Range and suggested that these histories are compatible with a rolling hinge model for the Snake Range décollement. Axen and Bartley (1997) evaluated the rolling hinge model from the perspective of field relations, and also discussed data from the Snake Range.

During the two-stage Cenozoic history of the Snake Range, with initial extension in late Eocene–early Oligocene time followed by large-magnitude extension in Miocene time, the locus of active faulting in the Snake Range appears to have migrated from west to east, abandoning earlier portions of the fault system as evidenced by the cooling histories of higher temperature systems on the western flank of the range (Lee, 1995). It is also possible that fairly rapid eastward migration of faulting occurred during the younger Miocene event, but this migration is not resolvable with our new data because its time span is too short.

In the northern Snake Range, a large component of pure shear as well as differential vertical uplift is needed to explain the fabrics developed during deformation of footwall rocks (Lee et al., 1987) and ultimately the uplift, exhumation, and cooling of the range as documented by the fission-track data presented in this paper.

The three-step model shown in Figure 10 is modified after our initial interpretation of the Snake Range décollement as described by Gans et al. (1985) and honors the above considerations as well as the new data presented in this paper. The model ascribes the uniqueness of the northern Snake Range to the progressive rise of a large welt of hot crust during extension in Miocene time. We suggest that the previously thickened crust beneath the northern Snake Range (the result of Cretaceous thrust faulting; e.g., Armstrong, 1972; Coney and Harms, 1984; Miller and Gans, 1989) may have helped initiate and localize this instability, which could have been ultimately driven by a renewed pulse of magmatism and extension across the northern Basin and Range in Miocene time (Dumitru et al., 1997). During the rise of this extending welt of crustal rocks, possibly cored by Cenozoic magmas, the most active part of the northern Snake Range décollement migrated eastward with the changing locus of the margin of the rising welt (Fig. 10). The final domal configuration and the vertical uplift of the northern Snake Range relative to adjacent regions is also related to this rising welt, which resulted in the observed bending or doming and down-to-the-west faulting of the Snake Range décollement along the west side of the range. The cartoon depiction of this uplifted and extended welt of crustal rocks in plan view illustrates how its lateral boundaries may have led to development of the transverse structural zones and their associated sedimentary basins (Fig. 10).

The model depicted in Figure 10 suggests that the rise of the Snake Range metamorphic core complex could have been related to driving forces that originated deeper in the crust and likely played an active rather than a passive roll in the initiation and development of the metamorphic complex and its overlying detachment fault. The rolling hinge and isostatic bending models for core complex uplift, in contrast, interpret these complexes as the result of, or the response to, denudation of the upper crust by faulting. Our more speculative conclusion is that the northern Snake Range décollement may not be a normal fault, but rather a highly complex structural boundary developed above a rising and extending mass of hot crustal rocks, perhaps cored by buoyant Miocene

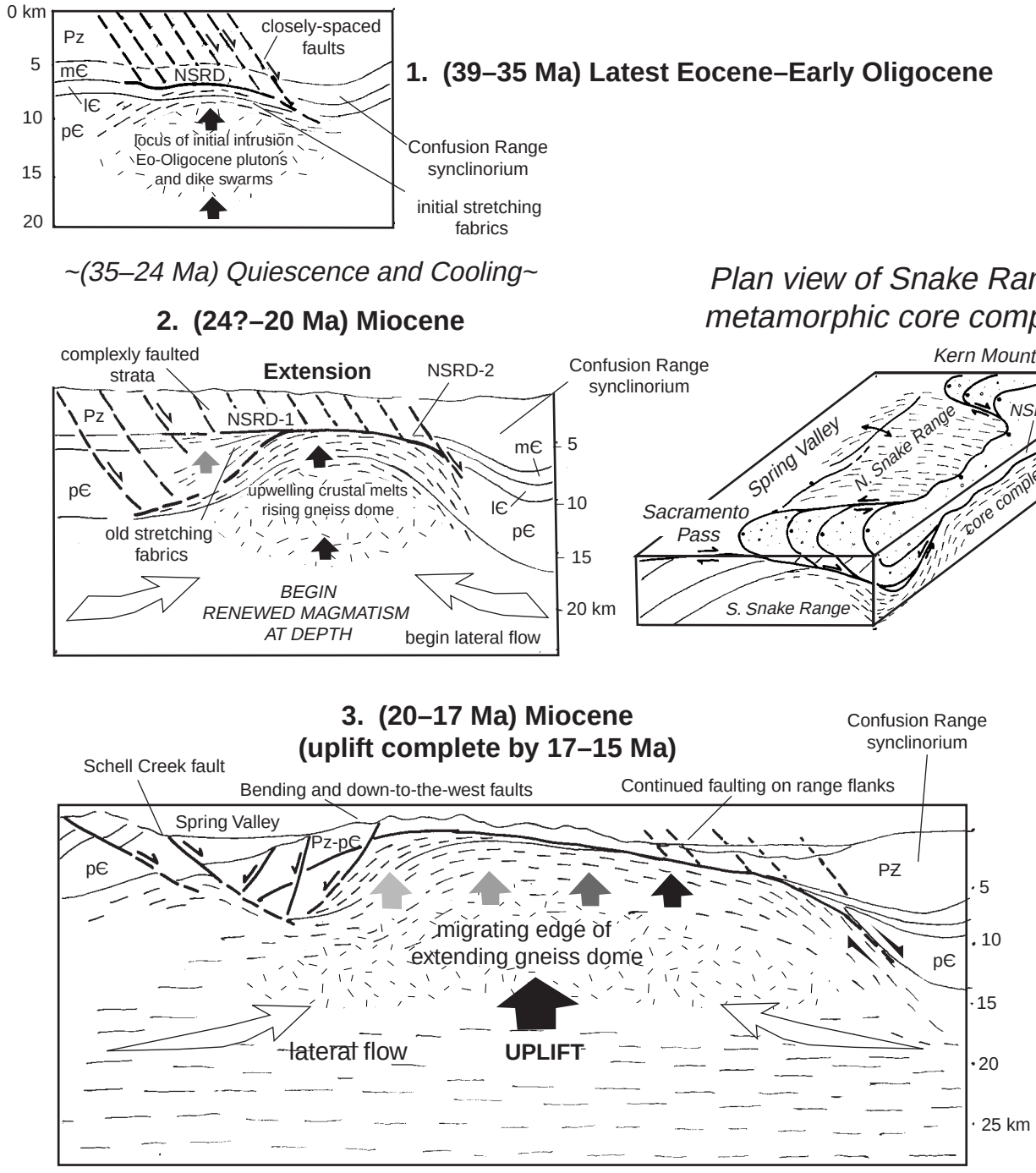

Figure 10. Model for the Cenozoic extensional and uplift history of the Snake Range, modified after Gans et al. (1985) to incorporate geologic and fission-track data discussed in this paper. For discussion, see text. NSRD—northern Snake Range décollement.

plutons and/or crustal melts. Analog modeling of extensional core complexes utilizing sand, silicone putty, and pods of low-viscosity materials (to reproduce the effects of granitic rocks or zones of partial melt) were carried out by Brun et al. (1994), who specifically remarked on the similarities of their models to the geometry of the northern Snake Range metamorphic core complex.

ACKNOWLEDGMENTS

Finalization of this manuscript and new data from the southern Snake Range and Schell Creek Range were partially funded by National Science Foundation grant EAR-9417939. Most of the data from the northern Snake Range in this paper were generated while Miller was a visitor at the Fission Track Laboratory at La Trobe University. Many thanks go to Andy Gleadow for his hospitality, insight, and input with this project. We also thank all of the working members of the laboratory at the time who answered our many questions and were always available to help. In particular, Dave Coyle, Dennis Arne, and Paul O'Sullivan were very helpful.

We thank all the past members of the Stanford Geological Survey for the hard work and energy and help in the preliminary stages of geologic mapping in east-central Nevada. Thanks also to Danny Stockli for collecting additional samples in the Schell Creek Range; Dean Miller for drafting and laboratory help; Keith Howard and Jeff Lee for reviewing early versions of the manuscript; and Gary Axen, Barbara Johns, and David Miller, who reviewed the submitted manuscript.

REFERENCES CITED

Armstrong, R. L, 1972, Low-angle denudational faults, hinterland of the Sevier orogenic belt, eastern Nevada and western Utah: Geological Society of America Bulletin, v. 83, p. 1729–1754.

Axen, G. J., and Bartley, J., 1997, Field tests of the rolling hinge hypothesis: Journal of Geophysical Research, v. 102, p. 20515–20537.

Bartley, J. M., and Wernicke, B. P., 1984, The Snake Range décollement interpreted as a major extensional shear zone: Tectonics, v. 3, p. 647–657.

Best, M. G., Armstrong, R. L., Graustein, W. C., Embree, G. F., and Ahlborn, R. C., 1974, Mica granites of the Kern Mountains pluton, eastern White Pine County, Nevada: Remobilized basement of the Cordilleran miogeosyncline?: Geological Society of America Bulletin, v. 85, p. 1277–1286.

Best, M. G., Christiansen, E. H., and Blank, H. R., Jr., 1989, Oligocene caldera complex and calc-alkaline tuffs and lavas of the Indian Peak volcanic field, Nevada and Utah: Geological Society of America Bulletin, v. 101, p. 1076–1090.

Brun, J.-P., Sokoutis, D., and Driessche, J. V. D., 1994, Analogue modeling of detachment fault systems and core complexes: Geology v. 22, p. 319–322.

Buck, W. R., 1988, Flexural rotation of normal faults: Tectonics, v. 7, p. 959–974.

Coney, P. J., 1979, Tertiary evolution of Cordilleran metamorphic core complexes, *in* Armentrout, J. M., Cole, M. R., and TerBest, H., Jr., eds., Cenozoic paleogeography of the western United States: Third Pacific Coast Paleogeography Symposium: Los Angeles, Pacific Section, Society of Economic Paleontologists and Mineralogists, p. 14–28.

Coney, P. J., and Harms, T. A., 1984, Cordilleran metamorphic core complexes: Cenozoic extensional relics of Mesozoic compression: Geology, v. 12, p. 550–554.

Corrigan, J. D., 1993, Apatite fission track analysis of Oligocene strata in south Texas, U.S.A.: Testing annealing models: Chemical Geology, v. 104, p. 227–249.

Davis, G. H., 1983, Shear-zone model for the origin of metamorphic core complexes: Geology, v. 11, p. 342–347.

Dumitru, T. A., 1990, Subnormal Cenozoic geothermal gradients in the extinct Sierra Nevada magmatic arc: Consequences of Laramide and post-Laramide shallow-angle subduction: Journal of Geophysical Research, v. 95, p. 4925–4941.

Dumitru, T. A., 1993, A new computer-automated microscope stage system for fission track analysis: Nuclear Tracks and Radiation Measurements, v. 21, p. 575–580.

Dumitru, T. A., 1999, Fission-track geochronology, in Noller, J. S., Sowers, J. M., and Lettis, W. R., eds., Quarternary geochonology: Applications in Quaternary geology and paleoseismology, V. 1: Washington, D., C., American Geophysical Union, Geophysical Monograph Series (in press).

Dumitru, T. A., Miller, E. L., Stockli, D. F., and Surpless, B. E., 1997, Fission track constraints on time-space patterns of Miocene extension in the northern Basin and Range Province: Geological Society of America Abstracts with Programs, v. 29, no. 6, p. 232.

Edwards, K., and Batson, R. M., 1990a, Experimental digital shaded-relief maps of Utah: U.S. Geological Survey Miscellaneous Investigations Map l-1847, scale 1: 1 000 000.

Edwards, K., and Batson, R. M., 1990b, Experimental digital shaded-relief maps of Nevada: U.S. Geological Survey Miscellaneous Investigations Map l-1849, scale 1:1 000 000.

Fitzgerald, P. G., Fryxell, J. E., and Wernicke, B. P., 1991, Miocene crustal extension and uplift in southeastern Nevada: Constraints from fission-track analysis: Geology, v. 19, p. 1013–1016.

Foster, D. A., Harrison, T. M., Miller, C. F., and Howard, K. A., 1990, The $^{40}Ar/^{39}Ar$ thermochronology of the eastern Mojave Desert, California, and adjacent western Arizona with implications for the evolution of metamorphic core complexes: Journal of Geophysical Research, v. 95, p. 20005–20024.

Galbraith, R. F., 1981, On statistical models for fission track counts: Mathematical Geology, v. 13, p. 471–478.

Galbraith, R. F., and Laslett, G. M., 1993, Statistical models for mixed fission track ages: Nuclear Tracks and Radiation Measurements, v. 21, p. 459–470.

Gans, P. B., and Miller, E. L., 1983, Style of mid-Tertiary extension in east-central Nevada, *in* Gurgel, K.D., ed., Geologic excursions in the overthrust belt and metamorphic core complexes of the intermountain region: Utah Geological and Mineral Survey Special Studies, v. 59, p. 107–160.

Gans, P. B., and Miller, E. L., 1985, The Snake Range décollement interpreted as a major extensional shear zone: Comment: Tectonics, v. 4, p. 411–415.

Gans, P. B., Miller, E. L., McCarthy, J., and Oldcott, M. L., 1985, Tertiary extensional faulting and evolving ductile-brittle transition zones in the northern Snake Range and vicinity: New insights from seismic data: Geology, v. 13, p. 189–193.

Gans, P. B., Mahood, G. A., and Schermer, E., 1989, Synextensional magmatism in the Basin and Range Province: A case study from the eastern Great Basin: Geological Society of America Special Paper 223, 53 p.

Gans, P. B., Miller, E. L., Clark, D. H., and Rodgers, D. W., 1990, Geologic relations in the Kern Mountains–Deep Creek Range, Nevada-Utah and the origin of metamorphic core complex detachment faults: Geological Society of America Abstracts with Programs, v. 22, no. 3, p. 24.

Gans, P. B., Miller, E. L., Brown, R., Houseman, G., and Lister, G. S., 1991, Assessing the amount, rate and timing of tilting in normal fault blocks: A case study of tilted granites in the Kern–Deep Creek Mountains, Utah: Geological Society of America Abstracts with Programs, v. 23, no. 2, p. 28.

Gans, P. B., Miller, E. L., Huggins, C. C., and Lee, J., 1999a, Preliminary geologic map of the Little Horse Canyon 7.5′ quadrangle, Nevada and Utah: Nevada Bureau of Mines and Geology Field Studies Map scale 1: 24 000 (in press).

Gans, P. B., Miller, E. L., and Lee, J., 1999b, Preliminary geologic map of the Spring Mountain 7.5′ quadrangle, northern Snake Range, Nevada-Utah: Nevada Bureau of Mines and Geology Field Studies Map, scale 1: 24 000 (in press).

Gleadow, A. J. W., Duddy, I. R., Green, P. F., and Lovering, J. F., 1986, Confined fission track lengths in apatite: A diagnostic tool for thermal history analysis: Contributions to Mineralogy and Petrology, v. 94, p. 405–415.

Green, P. F., 1981, A new look at statistics in fission track dating: Nuclear Tracks and Radiation Measurements, v. 5, p. 77–86.

Green, P. F., 1989, Thermal and tectonic history of the East Midlands shelf (onshore UK) and surrounding regions assessed by apatite fission track analysis: Geological Society of London Journal, v. 146, p. 755–774.

Green, P. F., Duddy, I. R., Gleadow, A. J. W., and Lovering, J. F., 1989a, Apatite fission-track analysis as a paleotemperature indicator for hydrocarbon exploration, *in* Naeser, N. D., and McCulloh, T. H., eds., Thermal history of sedimentary basins: Methods and case histories: New York, Springer-Verlag, p. 181–195.

Green, P. F., Duddy, I. R., Laslett, G. M., Hegarty, K. A., Gleadow, A. J. W., and Lovering, J. F., 1989b, Thermal annealing of fission tracks in apatite, 4, Quantitative modelling techniques and extension to geological timescales: Chemical Geology, v. 79, p. 155–182.

Grier, S. P., 1983, Tertiary stratigraphy and structural history of Sacramento Pass in the Snake Range, Nevada: Geological Society of America Abstracts with Programs, v. 15, p. 403.

Grier, S. P., 1984, Alluvial fan and lacustrine carbonate deposits in the Snake Range: A study of Tertiary sedimentation and associated tectonism [M.S. thesis]: Stanford, California, Stanford University, 55 p.

Hamilton, W. B., 1988, Detachment faulting in the Death Valley region, California and Nevada: U.S. Geological Survey Bulletin 1790, p. 51–85.

Howard, K. A., and Foster, D. A., 1996, Thermal and unroofing history of a thick, tilted Basin-and-Range crustal section in the Tortilla Mountains, Arizona: Journal of Geophysical Research, v. 101, p. 511–522.

Huggins, C. C., 1990, Nature and timing of metamorphism in the Smith Creek area, northern Snake Range, Nevada [M.S. thesis]: Stanford, California, Stanford University, 92 p.

Huggins, C. C., and Wright, J. E., 1989, Superimposed Cretaceous and Tertiary metamorphism in the northern Snake Range, Nevada: Geological Society of America Abstracts with Programs, v. 21, p. A95.

Hurford, A. J., and Green, P. F., 1983, The zeta age calibration of fission track dating: Chemical Geology, v. 41, p. 285–317.

Jackson, J., and McKenzie, D., 1983, The geometrical evolution of normal fault systems: Journal of Structural Geology, v. 5. p. 471–482.

Jackson, J. A., and White, N. J., 1989, Normal faulting in the upper continental crust: Observations from regions of active extension: Journal of Structural Geology, v. 11, p. 15–36.

John, B. E., and Foster, D. A., 1993, Structural and thermal constraints on the initiation angle of detachment faulting in the southern Basin and Range, the Chemehuevi Mountains case study: Geological Society of America Bulletin, v. 105, p. 1091–1108.

John, B. E., and Howard, K., 1995, Rapid extension recorded by cooling age patterns and brittle deformation, Naxos, Greece: Journal of Geophysical Research, v. 100, p. 9969–9979.

Koch, P. S., Christie, J. M., Ord, A., and George, R. P. J., 1989, Effect of water on the rheology of experimentally deformed quartzite: Journal of Geophysical Research, v. 94, p. 13975–13996.

Laslett, G. M., Kendall, W. S., Gleadow, A. J. W., and Duddy, I. R., 1982, Bias in the measurement of fission track length distributions: Nuclear Tracks and Radiation Measurements, v. 6, p. 79–85.

Lee, D. E., Stacey, J. S. D., and Fisher, L., 1986, Muscovite-phenocrystic two-mica granites of NE Nevada are Late Cretaceous in age, *in* Shorter contributions to isotope research: U.S. Geological Survey Bulletin 1622, p. 31–39.

Lee, J., 1995, Rapid uplift and rotation of mylonitic rocks from beneath a detachment fault: Insights from potassium feldspar $^{40}Ar/^{39}Ar$ thermochronology, northern Snake Range, Nevada: Tectonics, v. 14, p. 54–77.

Lee, J., and Sutter, J. F., 1991, Incremental $^{40}Ar/^{39}Ar$ thermochronology of mylonitic rocks from the northern Snake Range, Nevada: Tectonics, v. 10, p. 77–100.

Lee, J., Miller, E. L., and Sutter, J. F., 1987, Ductile strain and metamorphism in an extensional tectonic setting: A case study from the northern Snake Range, Nevada, U.S.A., *in* Coward, M. P., Dewey, J. F., and Hancock, P. L., eds., Continental extensional tectonics: Geological Society [London] Special Publication 28, p. 267–298.

Lee, J., Gans, P. B., and Miller, E. L., 1999a, Preliminary geologic map of the Mormon Jack Pass 7.5′ quadrangle, northern Snake Range, White Pine County, Nevada: Nevada Bureau of Mines and Geology Field Studies Map, scale 1: 24 000 (in press).

Lee, J., Gans, P. B., and Miller, E. L., 1999b, Preliminary geologic map of the Third Butte East 7.5′ quadrangle, northern Snake Range, White Pine County, Nevada: Nevada Bureau of Mines and Geology Field Studies Map, scale 1: 24 000 (in press).

Lee, J., Miller, E. L., Gans, P. B., and Huggins, C. C., 1999c, Preliminary geologic map of the Mount Moriah 7.5′ quadrangle, northern Snake Range, White Pine County, Nevada: Nevada Bureau of Mines and Geology Field Studies Map, scale 1: 24 000 (in press).

Martinez, C. M., Miller, E. L., and Stockli, D. F., 1998, Miocene age rock avalanche deposits of the Sacramento Pass Basin, Basin and Range Province, Nevada: Geological Society of American Abstracts with Programs, v. 30, no. 5, p. 53.

McGrew, A. J., 1993, The origin and evolution of the Southern Snake Range décollement, east-central Nevada: Tectonics, v. 12, p. 21–34.

McGrew, A. J., and Miller, E. L., 1995, Geologic map of Kious

Spring and Garrison 7.5′ quadrangles, White Pine and Millard Counties, Nevada and Utah: U.S. Geological Survey Open-File Report OF-95-10, scale 1: 24 000.

Miller, D. D., Miller, E. L., Stockli, D., Chan, C., Green Nylen, N., Hessler, A., Jaen, I., Lenkeit, A., Lucks, M., and Soria, A., 1995, Sedimentary record of Tertiary extension, Sacramento Pass area, Snake Range, east-central Nevada: Geological Society of America Abstracts with Programs, v. 27, no. 6, p. 389.

Miller, E. L., and Gans, P. B., 1989, Cretaceous crustal structure and metamorphism in the hinterland of the Sevier thrust belt, western U.S. Cordillera: Geology, v. 17, p. 59–62.

Miller, E. L., and Gans, P. B., 1999, Preliminary geologic map of The Cove 7.5′ quadrangle, northern Snake Range, White Pine County, Nevada: Nevada Bureau of Mines and Geology Field Studies Map, scale 1: 24 000 (in press).

Miller, E. L., and Grier, S. P., 1995, Geologic map of Lehman Caves 7.5′ quadrangle, White Pine County, Nevada: U.S. Geological Survey Map GQ-1758, scale 1:24 000.

Miller, E. L., Gans, P. B., and Garing, J., 1983, The Snake Range décollement: An exhumed mid-Tertiary ductile-brittle transition: Tectonics, v. 2, p. 239–263.

Miller, E. L., Gans, P. B., Wright, J. E., and Sutter, J. F., 1988, Metamorphic history of the east-central Basin and Range Province: Tectonic setting and relationship to magmatism, *in* Ernst, W. G., ed., Metamorphic and tectonic evolution of the Western U.S. Cordillera (Rubey Volume VII): Englewood Cliffs, New Jersey, Prentice-Hall, p. 649–682.

Miller, E. L., Forrest, S., Gans, P. B., Snoke, A., Wright, J., and Wyld, S., 1994a, Granites and core complexes of the Great Basin, Field trip guidebook, trip #10: Eighth International Conference on Geochronology, Cosmochronology and Isotope Geology, Berkeley, California, June 1994.

Miller, E. L., Gans, P. B., and Grier, S. P., 1994b, Geologic map of Windy Peak 7.5′ quadrangle, White Pine County, Nevada: U.S. Geological Survey Open-File Map and Report OF94-687, scale 1:24 000.

Miller, E. L., Gans, P. B., and Stanford Geological Survey, Geologic maps of the Wheeler Peak and Minerva Canyon 7.5′ quadrangles, southern Snake Range, Nevada: U.S. Geological Survey Open-File Map and Report, scale 1: 24 000 (in press).

Miller, E. L., Gans, P. B., Grier, S. P., Huggins, C. C., and Lee, J., 1999, Preliminary geologic map of the Old Mans Canyon 7.5′ quadrangle, northern Snake Range, White Pine County, Nevada: Nevada Bureau of Mines and Geology Field Studies Map, scale 1: 24 000 (in press).

Misch, P., 1960, Regional structural reconnaissance in central-northeast Nevada and some adjacent areas: Observations and interpretations, *in* Guidebook to the geology of east-central Nevada: International Association of Petroleum Geology and Eastern Nevada Geological Society, Eleventh Annual Field Conference, Salt Lake City, Utah, p. 17–42.

Rodgers, D. W., 1987, Thermal and structural evolution of the southern Deep Creek Range, west-central Utah and east-central Nevada [Ph.D. thesis]: Stanford, California, Stanford University, 184 p.

Smith, D. L., Gans, P. B., and Miller, E. L., 1991, Palinspastic restoration of Cenozoic extension in the central and eastern Basin and Range Province at latitude 39–40 degrees, *in* Raines, G. L., Lisle, R. E., Schafer, R. W., and Wilkinson, W. H., eds., Geology and ore deposits of the Great Basin: Reno, Geological Society of Nevada, p. 75–86.

Smith, M. J., and Leigh-Jones, P., 1985, An automated microscope scanning stage for fission track dating: Nuclear Tracks and Radiation Measurements, v. 10, p. 395–400.

Tagami, T., and Dumitru, T. A., 1996, Provenance and thermal history of the Franciscan accretionary complex: Constraints from zircon fission track thermochronology: Journal of Geophysical Research, v. 101, p. 11,353–11364.

Tullis, J., 1990, Experimental studies of deformation mechanisms and microstructures in quartzo-feldspatic rocks, *in* Barber, D. J., and Meredith, P. G., eds., Deformation processes in minerals, ceramics, and rocks: London, Unwin Hyman, p. 190–227.

Wdowinski, S., and Axen, G. J., 1992, Isostatic rebound due to tectonic denudation: A viscous flow model of a layered lithosphere: Tectonics, v. 11, p. 303–315.

Wernicke, B., 1985, Uniform-sense normal simple shear of the continental lithosphere: Canadian Journal of Earth Sciences, v. 22, p. 108–125.

Wernicke, B., 1995, Low-angle normal faults and seismicity: A review: Journal of Geophysical Research, v. 100, p. 20159–20174.

Wernicke, B., and Axen, G. J., 1988, On the role of isostasy in the evolution of normal fault systems: Geology, v. 16, p. 848–851.

MANUSCRIPT RECEIVED BY THE SOCIETY JUNE 13, 1997
REVISED MANUSCRIPT RECEIVED JUNE 23, 1998
MANUSCRIPT ACCEPTED AUGUST 25, 1998

Printed in U.S.A.